UCRL-51620

PROJECT DIAMOND ORE, PHASE IIA: CLOSE-IN MEASUREMENTS PROGRAM

Clyde J. Sisemore
Donald E. Burton
Jon B. Bryan

August 28, 1974

Prepared for U.S. Atomic Energy Commission under contract No. W-7405-Eng-48

LAWRENCE LIVERMORE LABORATORY

University of California/Livermore

Printed in the United States of America
Available from
National Technical Information Service
U. S. Department of Commerce
5285 Port Royal Road
Springfield, Virginia 22151
Price: Printed Copy $___*; Microfiche $1.45

*Pages	NTIS Selling Price
1-50	$4.00
51-150	$5.45
151-325	$7.60
326-500	$10.60
501-1000	$13.60

TID-4500, UC-35
Peaceful Applications
of Explosions

LAWRENCE LIVERMORE LABORATORY
University of California/Livermore, California/94550

UCRL-51620

PROJECT DIAMOND ORE, PHASE IIA: CLOSE-IN MEASUREMENTS PROGRAM

Clyde J. Sisemore
Donald E. Burton
Jon B. Bryan

MS. date: August 28, 1974

Contents

PROJECT DIAMOND ORE, PHASE IIA: CLOSE-IN MEASUREMENTS PROGRAM

Abstract

Project Diamond Ore was designed to determine the effects of stemming, depth of burial, and geology on nuclear and high explosive cratering phenomena. Phase IIA included three multiton chemical explosive cratering events. The close-in instrumentation for these events provided data to further code development work and to determine detonation histories. The instrumentation plan and emplacement procedures are described, and the recorded waveforms are reported, summarized, and interpreted in detail.

Introduction

The overall objective of Project Diamond Ore was to determine (1) the effects on crater dimensions of different types of stemming, of different depths of burial (DOB), and of different geologic media, and (2) the collateral effects of a subsurface nuclear detonation. Chemical explosive cratering detonations designed to model nuclear detonations were used.

Project Diamond Ore was jointly funded by the Defense Nuclear Agency (DNA) and the Office of the Chief of Engineers (OCE), U.S. Army, with program management provided by the U.S. Army Engineer Waterways Experiment Station Explosive Excavation Research Laboratory (EERL).

In October 1971, a series of multiton cratering experiments was conducted at Fort Peck, Montana, as Phase IIA of Project Diamond Ore. Three cratering charges, each having ~9000 kg of sand-contaminated slurry explosive, were detonated. Two of these detonations were at a DOB of 12.5 m with one detonation unstemmed (DOIIA-1) and one detonation stemmed (DOIIA-2). The third detonation (DOIIA-3) had a DOB of 6 m and was stemmed.

These experiments were conducted by EERL with participation from the Chemistry Department, Lawrence Livermore Laboratory (LLL); K Division, LLL; Systems, Science, and Software, Inc.; and the Operations Evaluation Department, Stanford Research Institute (SRI). The Chemistry Department, LLL, was responsible for explosive testing and for determining the detonation characteristics of the explosives considered. K Division, LLL; Systems, Science, and Software, Inc.; and EERL were responsible for the calculation efforts.

These detonations were highly instrumented by K Division to provide data for the code development work being conducted by LLL and Systems, Science, and Softwares, Inc. The SOC code provides a numerical solution to the propagation of a stress wave of arbitrary amplitude through a Lagrangian grid in one space dimension (spherical symmetry). The code has been structured to accept material properties data from a preshot testing program in order to predict the stress-induced effects on a rock mass caused by an explosive source. The code calculates stress, particle velocity and displacement history, cavity radius, extent of brittle failure, and the rock's efficiency for transmitting stress.[1] The detonations were also to provide a first look at the effects of stemming in multiton yields. The explosive equation-of-state (EOS) testing had not been completed by the time the Phase IIA detonations were conducted. The charge designs were therefore based on the energy test data provided by the manufacturer, and the explosive charges in Phase IIA were instrumented to verify and improve that data.

This report presents the results of the LLL instrumentation program.

Other measurements and technical programs conducted by other participants were directed toward comparing the effects of different stemming plans and DOB's on the resulting craters and determining collateral effects. These measurement programs included high-speed photography of each detonation, airblast measurements, ground shock measurements, and preshot and postshot aerial mapping of the craters. Their results are reported in Ref. 2.

Instrumentation

Close-in measurements were planned to provide the required data for code development and verification and to determine the detonation history of the explosive. The requirements for the close-in code verification measurements were developed by LLL and Systems, Science, and Software, Inc. The objective was to obtain the following data:

- HE performance
- Impulse coupling
- Shock wave attenuation
- Shock wave and surface interaction
- Surface motion
- Stemming performance
- Open hole gas flow.

To obtain this data, the following parameters were measured:

- Detonation velocity
- Shock velocity
- Particle velocity
- Surface velocity
- Peak detonation pressure
- Stress history
- Particle acceleration
- Surface acceleration.

Appendix A details the instrumentation used.

These stress and motion measurements were taken within and adjacent to the predicted crater during crater formation. The resulting stress and velocity

levels could then be compared directly with the calculated predictions for that detonation. Figures 1 through 3 show the linear array of close-in instrumentation used for each Phase IIA detonation. A close-in subsurface instrumentation program was not conducted on the 6-m detonation because similar data would be available from the 12.5-m stemmed detonation.

Figure 4 is a topographic map showing the general site layout for the Phase IIA experiments. The LLL Recording Trailer Park (RTP) No. 1 was used for the DOIIA-1 and DOIIA-2 detonations and the RTP No. 2 was used for the DOIIA-3 detonation. The Control Point (CP) and camera station remained in the same location for all three detonations. Cables were run directly from the RTP's to each SGZ.

Instrumentation holes were drilled at the locations shown in Figs. 1 through 3. Instrumentation packages were mounted on plastic pipe and aligned in each instrument hole. The instrument holes were then grouted with an LLL instrumentation grout commonly used at the Nevada Test Site. Surface motion instruments were placed in formed holes, which were then filled with ready-mix concrete. The surfaces of these grout pads were color-coded for postshot identification. All rate sticks and boosters were emplaced before the cavity was filled with explosive. Cables from each rate stick were placed against the cavity wall to ensure that they were not destroyed by the detonation before the pin closure signals were transmitted.

The access holes for the DOIIA-2 and DOIIA-3 detonations were stemmed in successive layers after each cavity had been loaded with explosives. The 1.22 m diam portion of the Diamond Ore IIA-1 access hole was stemmed to 0.91 m with the same Shotcrete used to shape the explosive cavities (see Fig. 5). See Appendix B for additional information on emplacement.

Data Summaries and Interpretation

The instrumentation provided information on detonation velocity, shock velocity, surface motions, stress history, particle velocity, and acceleration. Not only did this data allow verification of the SOC calculations, it provided information for evaluating explosive performance, correlating measurements, describing ground surface motion, defining soil attenuation characteristics, and determining HE gas velocities. The data is summarized and interpreted here; Appendix C reports the complete data.

TIME OF SHOCK ARRIVAL MEASUREMENTS (TOA)

In the Diamond Ore Phase IIA experiments, arrival times of the shock wave were measured principally in four regions: (1) within the aluminized ammonium nitrate slurry explosive, (2) along the shot horizon, (3) along the ground surface, and (4) within and adjacent to the emplacement hole of the 12.5-m unstemmed shot. Although most of the TOA data was a by-product of other types of instrumentation, rate sticks and

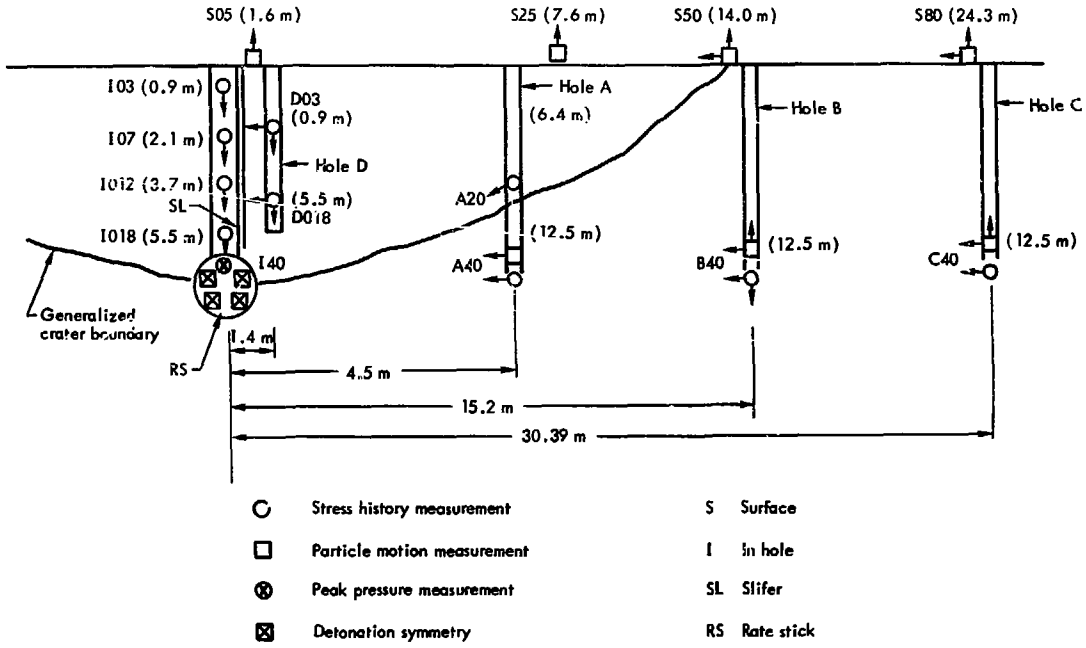

Fig. 1. Close-in instrumentation for DOIIA-1, 12.5 m, unstemmed.

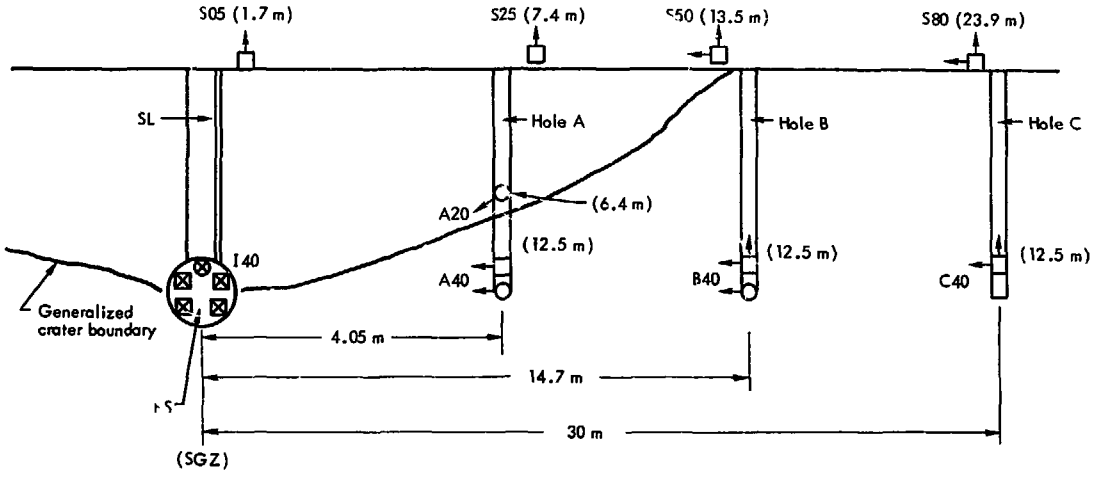

Fig. 2. Close-in instrumentation for DOIIA-2, 12.5 m stemmed. Cavity center offset ~0.457 m toward gages.

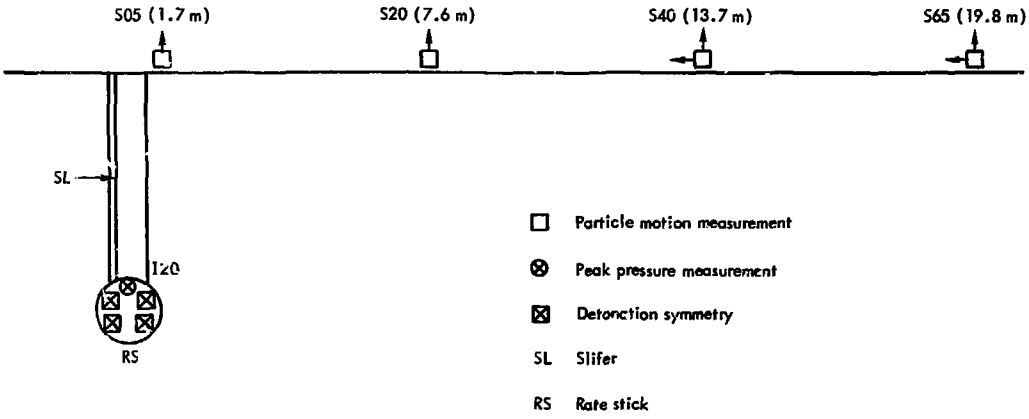

Fig. 3. Close-in instrumentation for DOIIA-3, 6 m, stemmed.

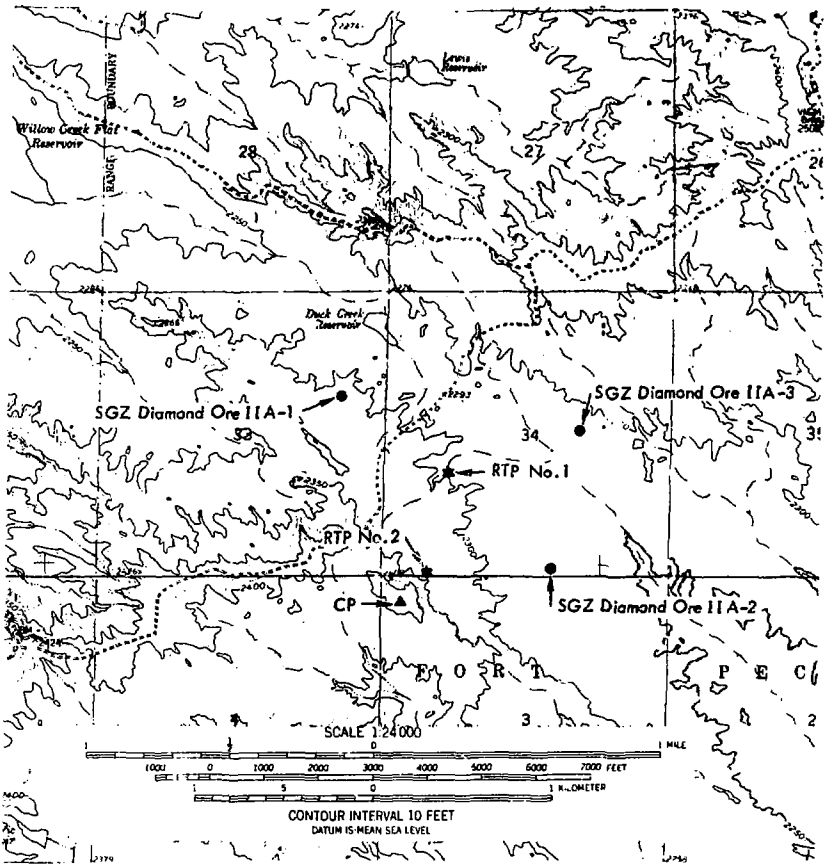

Fig. 4. Surface Ground Zero (SGZ), Control Point (CP), and Recording Trailer Park (RTP) locations.

slifers were emplaced specifically to provide arrival time data.

Detonation Velocity Measurements

Rate sticks (described in Appendix A) were placed in each HE sphere to measure detonation velocities. This data was then used to evaluate explosive performance. Arrival times and pin distances are displayed in Fig. 6. In all three events, rate sticks 1 and 2 were in the upper charge hemisphere, and 3 and 4 in

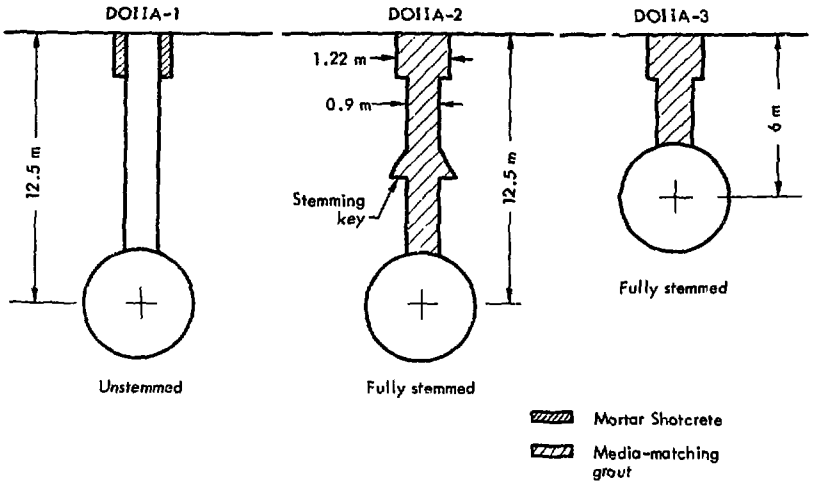

Fig. 5. DOIIA stemming configurations.

the lower hemisphere. Table 1 lists the asymptotic (late-time) detonation velocities for each rate stick.

For the DOIIA-1 shot (12.5 m, unstemmed), the observed detonation velocities closely match the preshot estimate of 5.3 m/ms. In Fig. 6, the slopes of the lines and not their relative placement should be considered. For example, the apparent displacement of the rate stick 1 data relative to the other three can then be interpreted either as a true asymmetry in the detonation or as a consequence of an erroneous signal identification. Positive identification of the signals is not always possible, because the signals from the piezoelectric pins are indistinguishable and because all pins did not report within the time frame of the oscilloscope trace.

The recorded velocities for the DOIIA-2 shot (12.5 m, stemmed) are clearly less than half those for the DOIIA-1 shot. The early signals from rate stick 1 suggest either a detonation wave front in the HE or an overdriven shock wave from the booster. The late-time velocities are comparable to the estimated sonic velocity of the explosive, implying that the detonation wave, if occurring at all, was considerably retarded.

In the DOIIA-3 shot (6 m, stemmed), rate sticks 1 and 4 failed prior to detonation. The failure has been attributed to the corrosive action of the slurry upon either cable connections or the diode circuit boards. The remaining rate sticks indicated considerable variations in the detonation characteristics between the

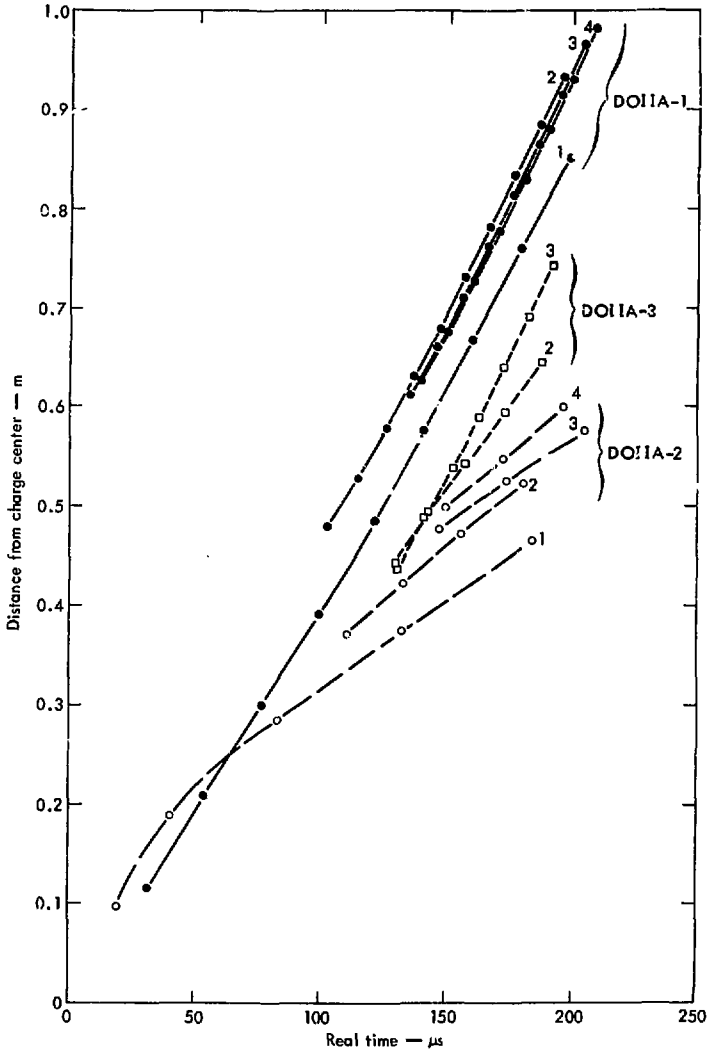

Fig. 6. Detonation arrival times for slurry explosive detonations in Phase IIA. Numbers are rate stick numbers.

Table 1. Summary of shock and detonation velocity measurements.[a]

	DOHA-1 12.5 m, unstemmed			DOHA-2 12.5 m, stemmed			DOHA-3 6m, stemmed		
	Source	Velocity (m/ms)	Remarks	Source	Velocity (m/ms)	Remarks	Source	Velocity (m/ms)	Remarks
Asymptotic detonation velocity in HE	RS1	4.72	Top	RS1	1.75	Top	RS1	–	Top
	RS2	5.10	Top	RS2	2.15	Top	RS2	3.31	Top
	RS3	5.18	Bottom	RS3	1.73	Bottom	RS3	5.20	Bottom
	RS4	5.13	Bottom	RS4	2.15	Bottom	RS4	–	Bottom
Shot level in Bearpaw shale	A, B, C	2.00 ± 0.04		A, B, C	2.00 ± 0.05				
	Seismic	1.5	Preshot	Seismic	1.8	Preshot	Seismic	1.1	Preshot
	HS	1.8	Long range	HS	1.6	Long range	HS	1.7	Long range
Surface	S	0.77 ± 0.05		S	1.07 ± 0.08		S	0.64 ± 0.07	
	Seismic	0.82	Preshot average	Seismic	0.81	Preshot average	Seismic	0.61	Preshot average
Emplacement hole	SL	~3.4	Air	SL	1.7	Grout	SL	1.3	Grout
	I	3.4 ± 0.1	–			–			
Air shock	HS	0.77	Near SGZ	–			HS	0.36	Near SGZ
	HS	0.33	Long range	–			HS	0.34	Long range

[a]RS = rate stick; A, B, C = instrument hole gages; HS = high-speed photography; S = surface gages, SL = slifer; I = emplacement hole gages.

upper and the lower hemisphere, with the latter detonating properly.

The rate stick data thus gives direct evidence of anomalous detonations in the two stemmed events. The results of the peak pressure measurements in the 12.5-m shots support this conclusion.

A number of possible causes for the erratic behavior of the explosive have been considered:

- Possible failures related to stemming. Stemming procedures were examined because the two stemmed detonations produced erratic results and the unstemmed detonation appeared to behave properly.

The method of backfilling the 0.91 m diam emplacement holes was to pour a density matching cement grout down the emplacement hole, using a canvas pipe. A piece of plywood was placed on top of the explosive to prevent the falling grout from penetrating. One possible mode of failure is penetration of the stemming material into the explosive at various points, creating discontinuities that could produce erratic initiation in the explosive.

Another possible stemming-related failure is induced densification of the explosive. Since slurry explosives will not initiate unless specific porosity levels are maintained, the combined weight of the explosive and the stemming material could cause appreciable density changes in the HE, resulting in erratic behavior.

- Possible failures related to explosive performance. It is possible that the detonator-booster may have failed to generate the necessary initiation pressures. Another and more likely cause of erratic HE performance is failure of the explosive to initiate reliably. The HE as designed may have been on the ragged edge of failure. If so, the sand contamination, a variation in chemical composition, a variation in particle size, a

Table 2. Recorded arrival times.

Gage location	DOHA-1 12.5 m, unstemmed				DOHA-2 12.5 m, stemmed				DOHA-3 6 m, stemmed			
	Station	Distance (m)	Gage[a]	TOA (m/s)	Station	Distance (m)	Gage[a]	TOA (m/s)	Station	Distance (m)	Gage[a]	TOA (m/s)
Shot level	A40	4.51	AC-R	1.64	A40	4.05	AC-R	1.88	–	–	–	–
			ST-R	1.58			ST-R	1.48				
	A20	7.59	ST-R	3.32	A20	7.31	ST-R	3.55	–	–	–	–
	B40	15.15	VE-R	–	B40	14.72	AC-T	7.0	–	–	–	–
			BE-T	7.5			VE-R	7.7				
			ST-R	6.9			ST-R	6.9				
			ST-T	7.1			ST-T	7.1				
	C40	30.39	AC-T	–	C40	29.86	AC-T	14.6	–	–	–	–
			VE-R	14.5			VE-R	–				
			STR-R									
Surface	S05	12.59	AC-V	8.34	S05	12.62	AC-V	9.32	S05	6.22	AC-V	3.20
	S25	14.60	VE-V	12.5	S25		VE-V	–	S20	9.69	AC-V	5.6
	S50	18.75	VE-V	18	S50	18.41	VE-V	–	S40	14.97	VE-V	–
			AC-HR	18.1			AC-HR	17.6			VE-HR	–
	S80	27.34	AC-V	27.1	S80	26.97	AC-V	22.9	S65	20.66	AC-V	25.0
			AC-HR	28.9			AC-HR	23.1			AC-HR	25.7
Emplacement hole	I40	1.1	P	0.24	I40	–	P	–	I40	–	P	–
	I18	7.01	ST-R	1.91								
	I12	8.88	ST-R	2.15								
	I07	10.36	ST-R	2.86								
	I03	11.58	ST-R	3.28								
Hole D	D18	6.65	ST-V	2.95								
			ST-HR	3.05								
	D03	11.36	ST-V	–								
			ST-HR	6.4								

[a]AC = accelerometer; HR = horizontal radial; VE = velocity gage; ST = stress gage; STR = strain gage; P = pressure; V = vertical; R = radial; T = tangential.

variation in porosity, or any other inhomogeneity could produce very erratic performance.

Since the Diamond Ore experiments, a large number of laboratory experiments have been designed to establish the cause or causes of failure; their results will be presented in a future report.

Shot Horizon TOA Measurements

This data was used to correlate measurements and to verify the constitutive relations for the SOC code one-dimensional calculations.[1] Arrival times were recorded with the stress, velocity, and acceleration gages emplaced in instrument holes A, B, and C for the stemmed and unstemmed 12.5-m events. The data is given in Table 2 and plotted in Fig. 7. No shot level measurements were made on the stemmed 6-m event.

The observed shock velocities of 2.00 m/ms (see Table 1) agree closely with those observed in the Pre-Gondola I experiments[3] but are considerably higher than these suggested by the preshot seismic refraction surveys (see Fig. 8). The Bearpaw clay shale constitutive relations as developed from the Pre-Gondola data[4] give a calculated shock velocity of 1.96 m/ms, in good agreement with the measured result.

Surface TOA Measurements

This data was used to correlate measurements, to describe the motion of the ground surface above the detonation, and to relate the SOC calculations to the observed surface motion. The observed surface station arrival times for the three events are also recorded in Table 2 and plotted in Fig. 7.

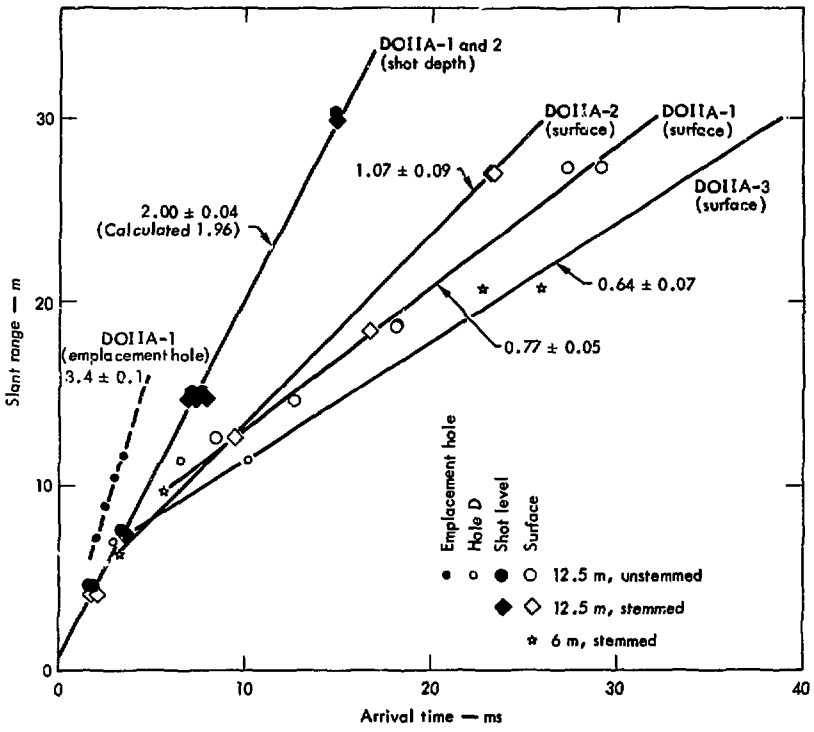

Fig. 7. Time-of-arrival data.

The noncoincidence of the surface arrival times curves for the different shots indicates substantial variation in the constitutive properties of the upper geologic layers. This is also supported by the preshot boring logs and seismic refraction surveys. Some refraction is clearly evident because the curves do not pass through the origin. In spite of this refraction, the slope of the lines correlates well with the media-weighted seismic velocities estimated from the preshot seismic survey (see Table 1).

The surface TOA data is particularly valuable because it provides, via the Buckingham-Pi theorem,[5] an effective means of relating the observed surface velocities, stresses, and accelerations to the same quantities calculated at shot depth using the SOC code.

Emplacement Hole TOA Measurements

This data was used to determine the air shock velocity in the open hole and to describe the shock wave asymmetry

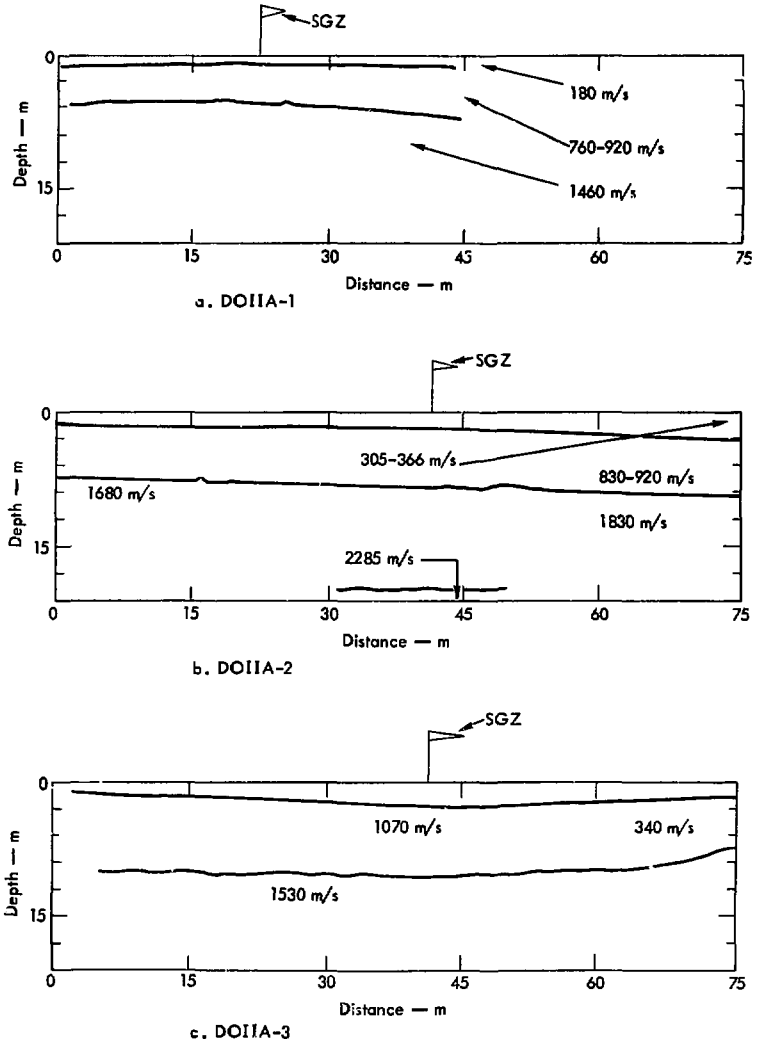

Fig. 8. Seismic refraction survey results for DOIIA surface ground zeros.

around the open hole. TOA data for the open emplacement hole of the 12.5-m unstemmed shot was obtained from four stress gages and one slifer located within the open hole. This data was supplemented by two pairs of stress gages located in an adjacent borehole (Hole D). Slifer systems were also placed in the grout stemming material of both stemmed events.

The shock velocities determined from the slifers in the open and grouted emplacement holes are recorded in Table 1. For the open emplacement hole of DOIIA-1, the slifer velocity (3.4 m/ms) is in complete agreement with that obtained from the stress gages. In the free atmosphere near SGZ, high-speed photography indicated that the air shock velocity had diminished from 3.4 m/ms to 0.77 m/ms.

Slifer velocities in the grouted emplacement holes were higher than the shock velocities in the undisturbed medium. This is supported by the high-speed photography data, which showed spallation occurring at the grout surface 1 to 2 ms before the surrounding Bear-paw shale surface. The failure to match grout and medium properties completely may have contributed to the stemming failures that occurred at 130 ms for DOIIA-2 and at 29 ms for DOIIA-3. These failures were, however, sufficiently late to have had negligible effect on the overall cratering process. The TOA data for the stress gages in Hole D (located parallel to but 1.43 m from the emplacement hole) does not offer a clear indication of whether the shock first reached these gages via the emplacement hole or through the soil. Consequently, we cannot use the TOA data to make any conclusions regarding shock wave asymmetries.

PRESSURE, STRESS, AND STRAIN MEASUREMENTS

We tried to measure the Chapman-Jouguet pressure of the explosive on all three events, using plastic gages. Stress history measurements were made on the 12.5-m unstemmed and 12.5-m stemmed experiments only. On these events, stress transducers were situated at shot level in Holes A and B and at half shot depth in Hole A. For the unstemmed event, four transducers were placed in the open emplacement hole and four more in Hole D. We attempted a strain measurement in Hole C, but the strain gage failed for some reason not yet determined.

Chapman-Jouguet Pressure

In all three events, plastic gages (described in Appendix A) were emplaced within the explosive and ~0.15 m from the top of the explosive surface (Stations 140 and 120). Of the three gages, only the gage in the DOIIA-1 detonation produced a satisfactory signal. Unfortunately, an error occurred in the preshot amplitude calibration for this channel and the amplitude may be in error. However, an experimental recording system was also being tested on this experiment. Data from this system was used to generate indirectly a postshot calibration. The peak pressure using this calibration is ~8 GPa (±20%).

This result supports the TOA data. The 8 GPa recorded for the unstemmed 12.5-m shot indicates that the HE performed as expected. For proper operation the stress pulse must rise above

5 GPa in less than 50 ns. Previous experience with the gage used has been very good; therefore, the absence of data from gages we knew to be working suggests either a low-amplitude pressure pulse or a very long rise time. Either of these indicates poor or erratic HE performance.

Shot-Level Stress History Measurements

Subsurface stress measurements were designed to verify the SOC code calculations and predictions of impulse transfer between the explosive and the surrounding soil and to define the attenuation characteristics of the soil.

Although signals were received from the surface-mounted voltage-controlled oscillators (VCO) for several hundred milliseconds, most subsurface stress gages failed to give correct stress histories for time intervals greater than a few milliseconds. In most cases, the recorded signal rose to a first peak and then flattened out or continued to rise discontinuously over several hundred milliseconds. As the shock front should be of only a very few milliseconds duration, this behavior is clearly impossible. The most likely cause of failure is a break in the signal circuit between the crystal and the surface-mounted shunt capacitor. A broken circuit would allow a constant capacitor voltage and therefore a constant signal. Abrupt decreases in the signal are caused by momentary grounding of this open circuit electronics system. Abrupt increases in the signal that occur after passage of the shock front can only be caused by a sudden change in the capacitive load of the electronics circuit.

In a few records, the first peak is followed by a slight decrease before flattening, suggesting that gage failure occurred upon release from peak load conditions. Since cable failure would be expected only after significant displacement of the gage, it seems likely that the cables would survive the initial shock loading. If we assume, then, that most of the gages or cables failed at or shortly after the peak, we can take the first peak as the peak amplitude of the shock wave at that location. Interpreted in this fashion, the peak stresses behave in a consistent manner (see Appendix C for individual signals). These values are tabulated in Table 3 and displayed graphically in Fig. 9.

In the case of the stress gages at stations A40 and I18 on the unstemmed event, a different type of failure occurred. Here the signal was driven rapidly downward during the onset of stress by a short-circuit that momentarily discharged the shunt capacitor. The peak values reported for these gages have been estimated by extrapolating the slopes prior to and following the short circuit.

The most prominent feature of Fig. 9 is the difference (by a factor of ~2) between the shot level stresses for the stemmed and unstemmed shots. Contrary to what might be expected, the stresses for the unstemmed shot are higher. We must assume that the known anomaly in the detonation of explosive for the stemmed shot is the source of the stress degradation seen in Fig. 9.

In an effort to determine the nature of the anomalous detonations, a suite of SOC calculations was performed using various Jones-Wilkins-Lee (JWL) explosive parameters.[6] The observed ground motion between the two shots did not differ

Table 3. Peak stress measurements.

Location	DOIIA-1 12.5 m, unstemmed				DOIIA-2 12.5 m, stemmed			
	Station	Distance (m)	Component[a]	Stress (GPa)	Station	Distance (m)	Component[a]	Stress (GPa)
Shot level	A40	4.51	R	>0.78	A40	4.05	R	0.34
	A20	7.59	R	0.50 ?	A20	7.31	R	0.15
	B40	15.15	R	0.21	B40	14.72	R	0.10
			T	0.21			T	0.14
	C40	30.39	R	–				
Emplacement hole	I40	~1.1	P	~8.0	I40		P	–
	I18	7.01	R	0.45 ?				
	I12	8.84	R	0.33				
	I07	10.36	R	0.10				
	I03	11.58	R	0.06 ?				
Hole D	D18	6.86	V	0.12				
			HR	0.13				
	D03	11.36	V	–				
			HR	0.028				

[a] R = radial; T = tangential; P = pressure; V = vertical; HR = horizontal-radial.

appreciably in spite of the disparity in the peak stress. This fact alone restricts the number of plausible explanations to those that would allow the shock energy to be spread over a broader front in the case of the stemmed event. The JWL formulation allows this time spread in energy by postulating a two-phase detonation wave. In the second phase, energy is released gradually over a finite time interval called the ramp time.

Peak radial stresses were calculated for two explosive sources. One has a ramp time of 50 μs (labeled A in Fig. 9) and the other has a ramp time of 2000 μs (labeled B in Fig. 9). The JWL parameters describing the explosive appear in Table 4. The agreement with the shot level gage results is quite good, and these calculations are taken to be the best theoretical estimates for the unstemmed and stemmed 12.5-m events. Since detonation anomalies were known to exist for the 6-m stemmed event and since there were no stress measurements to disprove this contention, estimates using calculation B will be assumed valid for the 6-m event.

Unstemmed Emplacement and Satellite Hole Stress Measurements

Four single crystal transducer systems were placed in the open emplacement hole of the unstemmed shot to measure the stress profile in the open

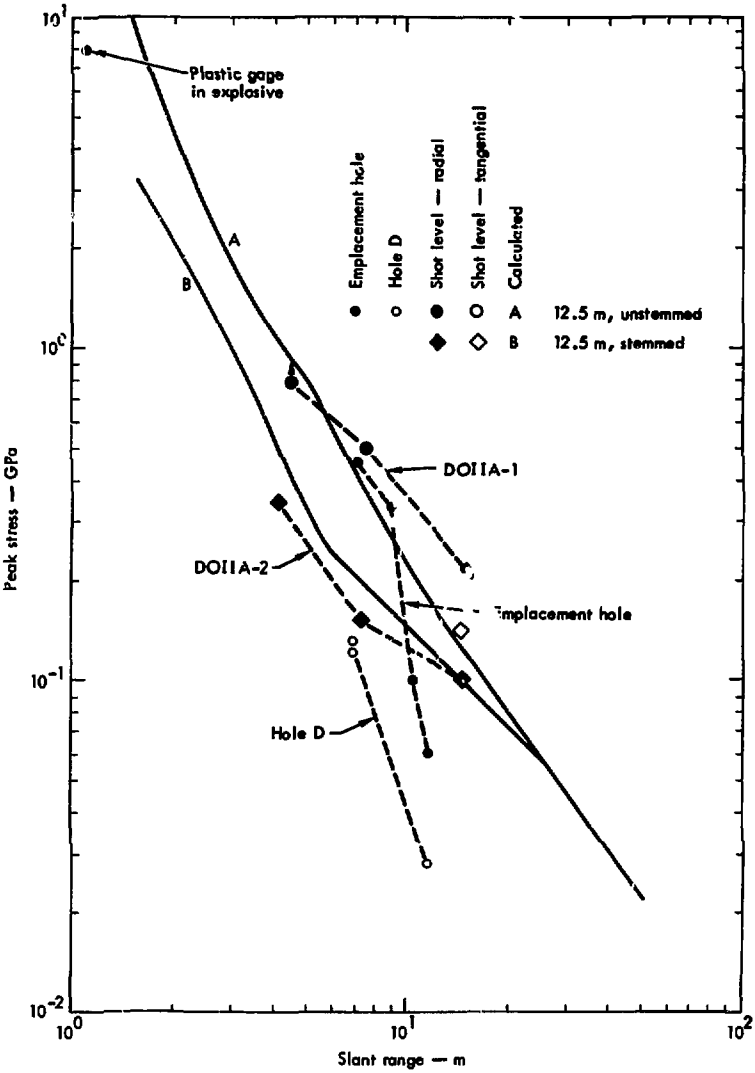

Fig. 9. Peak stress amplitudes.

Table 4. JWL parameters. From Ref. 7.

Pressure	$P(V, E, t) = [1 - F(t)]\, P_1(V, E) + F(t)\, P_2(V, E)$
	$P_i(V, E) = A_i\left(1 - \frac{\omega_i}{R_{1i}\rho_0 V}\right)e^{-R_{1i}\rho_0 V} + B_i\left(1 - \frac{\omega_i}{R_{2i}\rho_0 V}\right)e^{-R_{2i}\rho_0 V} + \frac{\omega_i E}{\rho_0 V}$
Ramp time	$F(t) = \begin{cases} t/\tau & 0 \le t \le \tau \\ 1 & t > \tau \end{cases}$

	JWL coefficients	Chapman-Jouguet state
Initial reaction	A_1 = 0.310073 TPa	ρ_0 = 1.5 Mg/m^3
	B_1 = 0.252 GPa	D = 5.3 km/s
	ω_1 = 0.25	P_{CJ} = 9.5 GPa
	R_{11} = 4.6	μ_{CJ} = 0.2941
	R_{21} = 1.4	E_0 = 2.6 GPa
Final reaction	A_2 = 0.57721 TPa	E_0 = 11 GPa
	B_2 = 0.85562 TPa	
	ω_2 = 0.45	
	R_{12} = 5.0	
	R_{22} = 1.4	

hole. Additional stress transducers were placed in Hole D to determine stress asymmetries around the open emplacement hole.

Data from the open hole stress transducers is shown in Fig. C-8 in Appendix C. Hole D data is shown in Appendix C (Figs. C-6 and C-7) and is summarized in Table 3 and Fig. 9. Although the signals were received for several milliseconds, the stress gages appear to have failed because of an open circuit between the gage and surface-mounted shunt capacitor. Because the gage at Station I18 shorted momentarily during rise, the reported peak value has been estimated by slope extrapolation. The peak values reported assume that failure occurred subsequent to maximum stress.

Both the horizontal and vertical stress gages at Station D18 in Hole D reported a relatively sharp spike at 3 ms (see Fig. C-6 in Appendix C). The narrow width of the spike suggests the signal source to be relatively small (e.g., the expanded gases in the emplacement hole). The lower values for peak stress measured in this hole plus the presence of the narrow spikes combine to show a significant amount of asymmetry around the emplacement hole.

ACCELEROMETER DATA

Accelerometers were placed at shot level on the two 12.5 m shots and at three surface locations on all three shots. The

subsurface gages were emplaced primarily as backup instrumentation for the stress history measurements, while the surface measurements were designed to verify code-predicted values of surface motion.

The accuracies of the peak acceleration determinations are limited to about ±25%. Accuracy is limited for the high frequency components by the filtering used in the playback system and for the low frequency components by the signal-to-noise ratio. Neither of these problems should affect the accuracy of the peak velocity determinations. The baseline shifts, however, are very critical, so much so that accuracies are very difficult to assign to the integrated velocities.

Shot-Level Accelerations

Because of the similarity between the stress measurement and accelerometer systems, we would anticipate a similar primary failure mode, that is, a break in the circuit between the gage and the surface-mounted shunt capacitor. The key indicator of this type of failure is a signal that becomes instantaneously constant and remains so for a relatively long period of time. Of the five shot-level accelerometers on the 12.5-m events, three failed in this manner, one failed preshot, and the last failed from causes presently unknown.

Surface Accelerations

All components of the surface accelerometer stations (accelerometer, shunt capacitor, and VCO) were mounted within the same instrument pad. Consequently, connecting cables were short and not subject to differential motion. This gave better survival conditions, and in no case did the surface gages fail in the same mode as the shot-level gages. In fact, no surface accelerometer failed completely, although several exhibited poor signal-to-noise ratio or baseline shifts due to permanent distortion of the crystal mounting or both.

The peak vertical and horizontal accelerations recorded at the surface stations are listed in Table 5, and plotted in Fig. 10. Figure 10 also shows three curves derived from SOC calculations for the peak vertical acceleration. Calculations A (12.5 m, unstemmed) and B (12.5 m, stemmed) are the same calculations discussed in connection with peak stress. Curve C is the same as B except for adjustments to correct for the 6-m DOB and arrival times. Because the SOC calculations included no ground surface interface and because they assumed homogeneous material, several corrections must be applied before making a comparison between calculational and experimental results. Vertical surface accelerations were derived from SOC calculations using

$$a_v(r) = \frac{2d}{r}\left(\frac{\tau}{\tau_c}\right)^2 a_c(r). \qquad (1)$$

The subscript c denotes calculated quantities; r is slant range. The vertical component of the calculated radial acceleration is obtained by multiplication by the ratio d/r (depth of burst to slant range). The factor of 2 arises because of the presence of the free surface. The ratio of observed to calculated shock arrival times (τ/τ_c) follows from the Buckingham-Pi theorem and represents a very significant correction at the larger

Table 5. Recorded peak accelerations.

Location	DOIIA-1 12.5 m, unstemmed			DOIIA-2 12.5 m, stemmed			DOIIA-3 6 m, stemmed		
	Station[a]	Distance (m)	Acceleration (m/s^2)	Station[a]	Distance (m)	Acceleration (m/s^2)	Station	Distance (m)	Acceleration (m/s^2)
Surface vertical	S05	12.59	40 000	S05	12.62	30 000	S05	6.22	120 000
	–	–	–	–	–	–	S20	9.69	34 500
	S80	27.34	620	S80	26.67	1 080	S65	20.66	740
Surface horizontal	S50	18.75	390	S50	18.41	980	–	–	–
	S80	27.34	235	S80	26.97	210	S65	20.66	290
Shot level	A40R	4.51	~200 000	A40R	4.05	~270 000			
	–	–	–	B40T	14.72	–			
	C40T	30.39	–	C40T	29.96	–			

[a] R = radial; T = tangential.

distances. The arrival times were taken from Fig. 7. The arrival time adjustment is an approximation, and it is used to correct for the effects of material layering on peak surface measurements, a factor not incorporated in the one-dimensional SOC calculations.

The accelerations calculated by SOC and adjusted as described are typically a factor of 2 greater than observed. One possible explanation lies in the rapid acceleration rise times and in the fact that the accelerometers were emplaced ~0.5 m below the top surface of the concrete instrument pad. Under these conditions, the recorded acceleration could peak before the arrival of the rarefaction from the pad surface. The factor of 2 in Eq. 1 would not then be justified because the observed peaks would actually represent free-field values. The records of the S05 accelerometers on the two 12.5-m events (Figs. C-11 and C-23) both display a double peak structure that tends to support this hypothesis.

PARTICLE VELOCITY DATA

Surface and subsurface particle velocity information was obtained from three types of observation: integrated accelerometer records, velocity gage records, and high-speed photography correlated with postshot target surveys.

Integrated Accelerometer Records

Of the shot-level accelerometers on the two 12.5-m events, only those at the A40 stations functioned long enough for their data to merit integration; even then, only minimum values for the peak velocities were obtainable.

Integration of the surface accelerometer records was hindered by baseline shifts and poor signal-to-noise ratios, which prevented observation of a definite gas-acceleration phase. The surface velocity measurements are consequently limited to the early-time spallation phase. Integration of records exhibiting pronounced baseline shifts was stopped after

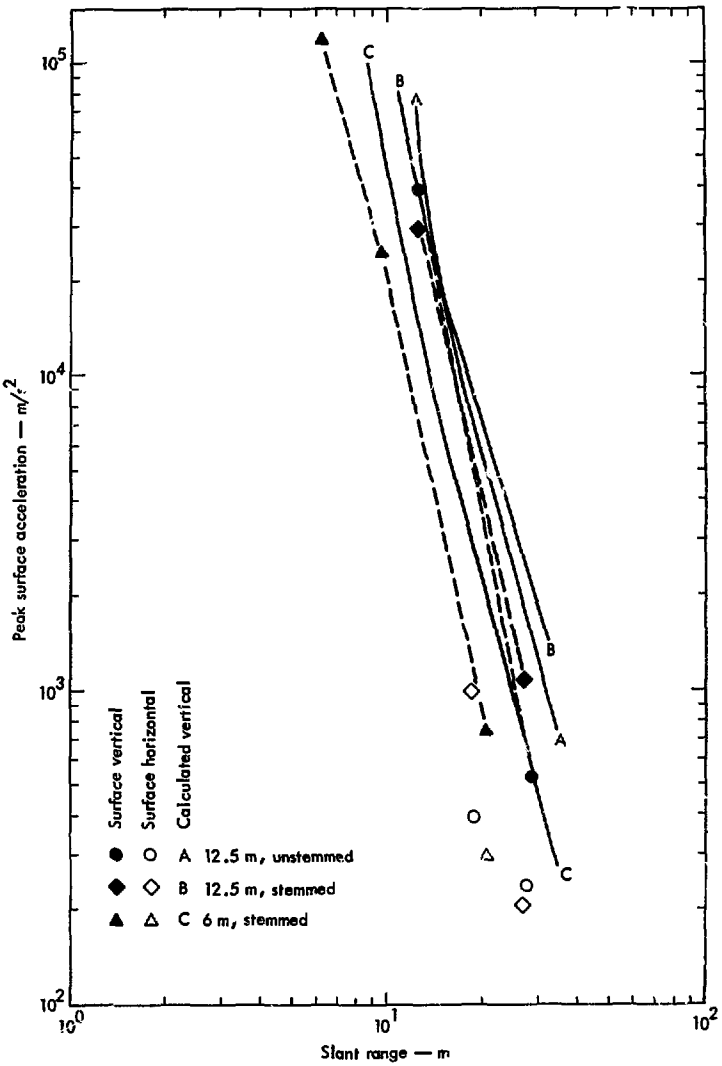

Fig. 10. Peak surface acceleration.

the signals had leveled off at constant values. The peak horizontal and vertical surface velocities obtained from the integrations appear in Table 6.

Velocity Gage Measurements

Particle velocity transducers were used at shot level on the 12.5-m events and at surface stations on all events. The overall performance of the velocity transducer systems was very poor. Of eleven systems, only three produced any usable data. Four failed prior to detonation, possibly because of water leakage. Two failed immediately upon shock incidence because of damage to the subcarrier or main carrier oscillator systems. Two continued to function but produced only spurious signals (see Appendix A).

Of the three usable signals, two survived only long enough to provide peak information before failure of the subcarrier oscillator. These were at stations S50 on DOIIA-1 and B40 on DOIIA-2. The remaining gage (S25 on DOIIA-1) survived for over 100 ms and provided a good signal. The peak particle velocities determined for these gages also appear in Table 6.

High-Speed Photography

The photography program fielded by EERL[2] included two high-speed cameras with framing rates of 1 to 2 ms per frame and a documentary type movie camera (~20 ms per frame). An additional high-speed camera was provided by the Dow Chemical Company for the DOIIA-1 event only. The surface motion targets were the concrete surface instrument and VCO pads, which had been color-coded for photographic and postshot identification. Time calibration was provided by 9.66 ms timing markers on one of the cameras. Distance calibration was based on three foreground reference targets placed at

Table 6. Recorded peak vertical and horizontal particle velocities.

	DOIIA-1 12.5 m, unstemmed				DOIIA-2 12.5 m, stemmed				DOIIA-3 6 m, stemmed			
Location	Station	Distance (m)	Gage	Velocity (m/s)	Station	Distance (m)	Gage	Velocity (m/s)	Station	Distance (m)	Gage	Velocity (m/s)
Surface vertical	S00	12.5	HS[a]	~60	S00	12.5	HS[a]	49	S00	6.	HS[a]	180
	S05	12.59	AC	50	S05	12.62	AC	58	S05	6.22	AC	>30
	A	13.	HS	~60	—						HS	160
	S25	14.6	VE	40[b]	S25	15.	VE	~	S20	8.5	HS	91
			HS	29			HS	37		9.69	AC	60[b]
	S50	18.75	VE	>14[b]	S50	18.41	VE	.	S40	14.97	VE	—
			HS	13			HS	18			HS	21
	B	20.	HS	11	B	20.	HS	15	--			
	S80	27.34	AC	6.4	S80	26.97	AC	7.0	S65	20.66	AC	7.0
Surface horizontal	A	13.	HS	~12			—		—			
	S25	14.6	HS	17	S25	15	HS	15	S20	8.5	HS	30
	S50	18.75	AC	5.6	S50	18.41	AC	5.	S40	14.97	VE	—
			HS	11			HS	11			HS	20
	B	20	HS	8	B	20	HS	8	—			
	S80	27.34	AC	3.9	S80	26.97	AC	2.1	S65	20.66	AC	4.0
Shot level	A40	4.51	AC-R	~	A40	4.05	AC-R	~				
	B40	15.15	VE-R	~	B40	14.32	VE-R	—				
			VE-T	—			AC-T	—				
	C40	30.39	VE-R	—	C40	29.96	VE-R	—				
			AC-T	—			AC-T	—				

[a]HS = data from high-speed photography; AC = accelerometer; VE = velocity gage; R = radial; T = tangential.

[b]Values estimated because of partial gage failure.

22.8 m intervals along a line displaced 61 m from SGZ toward the camera station.

The target spall velocities were found by two methods. The first involved fitting the observed vertical displacement to the ballistic equation to determine the initial velocity. The second involved the use of finite differences to deduce the early-time limit of the velocity. The results of these two techniques were found to be generally in agreement. Table 6 gives the results. Errors are estimated to be ~10%.

The horizontal components were found from the known postshot target displacement and the initial vertical velocity component by assuming the validity of the ballistic equation. Effects of air friction were ignored. The resulting peak horizontal target velocities are also in Table 6.

In addition to surface velocities, the photography program provided the necessary data to determine velocities and vent times of the high explosive gases. The unstemmed DOIIA-1 detonation vented within the first millisecond. The venting and the flash from the zero time flashbulb appeared in the same frame. This venting appears to have been interrupted by a possible closure of the access hole at ~90 ms. The stemming appears to have failed in the DOIIA-2 detonation at ~130 ms and at ~29 ms in the DOIIA-3 detonation. Failures at these late times are not thought to have had any significant effect on overall crater sizes. The hot spots or burning orange masses that appeared in the detonation cloud were observed on the photography. They are believed to have been masses of burning explosive. They appeared in the time frames as follows: DOIIA-1, 1.9 to 3.6 s; DOIIA-2, 4.0 to 8.5 s, and DOIIA-3, 0.4 to 7.9 s. Discussions with Dow Chemical Company representatives on the site indicated that these iridescent objects are common in the detonation of large quantities of this type of explosive.

The observed gas vent velocities were:

DOIIA-1	1500 m/s
DOIIA-2	180 m/s
DOIIA-3	450 m/s.

The very high vent velocity in the DOIIA-1 detonation results from the unstemmed emplacement hole. The difference in the vent velocities for the two stemmed cases is attributed to the earlier venting (29 ms) of the DOIIA-3 detonation, when the cavity pressure was higher. This earlier vent, in turn, resulted from the shallower DOB.

The peak vertical surface velocities of Table 6 have been plotted as a function of slant range in Fig. 11. As was indicated earlier, there is very little difference between the surface velocities of the two 12.5-m events. Three theoretical curves have also been included in the figure. These were obtained from SOC calculations and by using

$$V_v(r) = \frac{2d}{r}\left(\frac{\tau}{\tau_c}\right)V_c(r), \qquad (2)$$

in which the notation is similar to that used in determining surface accelerations. Here, V_c is the peak radial particle velocity calculated by SOC. In the case of the 12.5-m events, the agreement is remarkable. The theoretical results for the 6-m event are ~30% low. This difference can be explained by the large uncertainty in the arrival times at the surface stations, particularly S65.

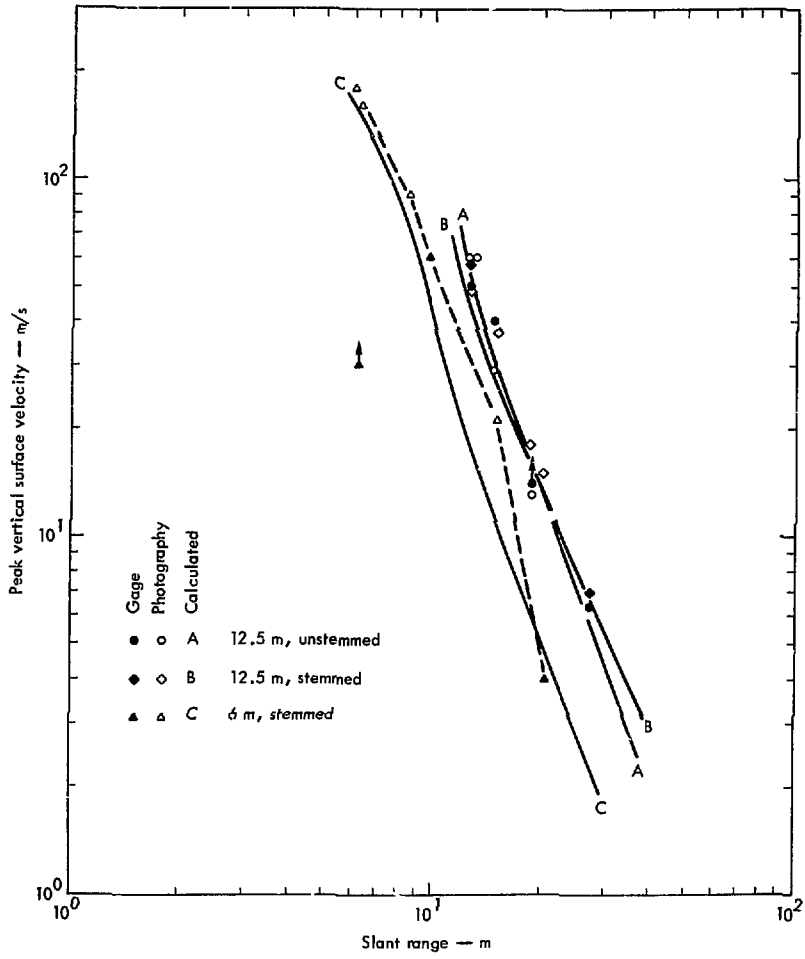

Fig. 11. Peak vertical surface velocity.

The peak horizontal surface velocity components have been plotted in Fig. 12. The three theoretical curves have been determined from

$$V_H(r) = \left[1 - \left(\frac{d}{r}\right)^2\right]^{1/2} \left(\frac{\tau}{\tau_c}\right) V_c(r). \quad (3)$$

The theoretical curves appear to be bounded near SGZ by the photographic data, which is 50 to 100% high. At greater ranges, the curves are bounded by the gage velocities, which are 50 to 100% low. No satisfactory explanation of this phenomenon has yet been found.

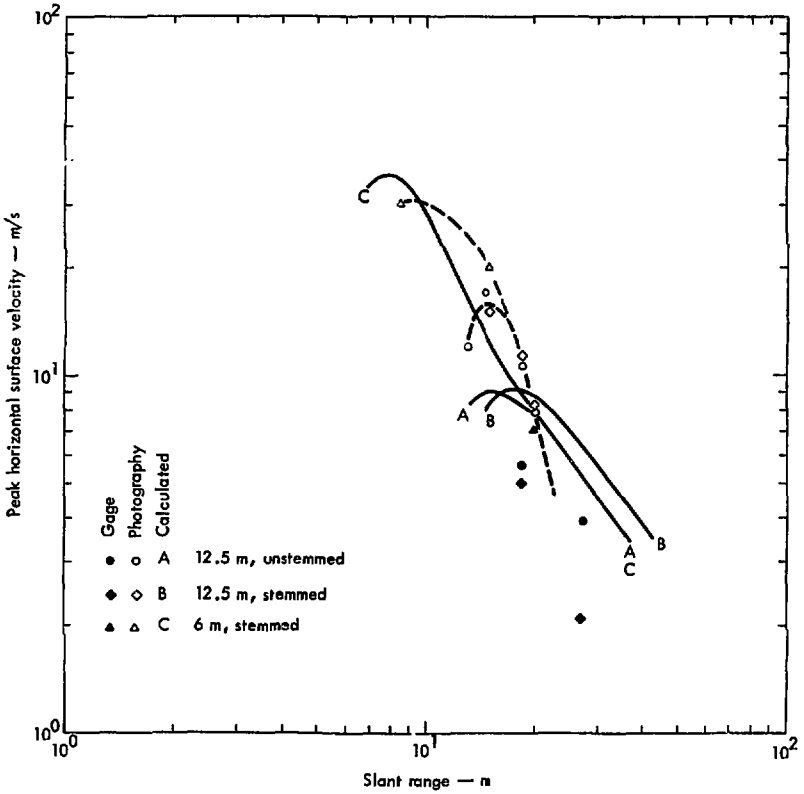

Fig. 12. Peak horizontal surface velocity.

Acknowledgments

We gratefully acknowledge valuable technical assistance in the following areas:

Planning, designing, and assembling the experimental hardware: S. Warner, N. W. Stewart.

Fielding and emplacing the experimental hardware: N. W. Stewart, C. P. Palmer, D. L. Wooster, R. M. Boat, J. M. O'Conner, R. L. Fraser, W. Wnuk.

Data recording: O. H. Krause, R. Ryan, A. Gusman.

Data analysis: M. D. Denny, M. Finger, O. H. Krause, E. L. Lee.

References

1. J. T. Cherry and F. L. Petersen, "Numerical Simulation of Stress Wave Propagation from Underground Nuclear Explosions," in Proc. ANS Symposium on Engineering with Nucl. Explo., Las Vegas, 1970 (American Nuclear Society, Hinsdale, Ill., 1970) CONF-700101, Vol. 1.
2. J. W. O'Connor, T. J. Donlan, and D. E. Burton, Explosive Selection and Fallout Simulation Experiments: Nuclear Cratering Device Simulation (Project Diamond Ore), U.S. Army Engineer Waterways Experiment Station Explosive Excavation Research Laboratory, Livermore, Calif., Rept. TR E-73-102 (1973).
3. J. D. Day, D. W. Murrill, and W. C. Sherman, Close-in Ground Motion, Earth Stress, and Pore Pressure Measurements, U.S. Army Engineer Nuclear Cratering Group, Livermore, Calif., Rept. PNE-1104 (1968).
4. B. K. Crowley, D. E. Burton, and J. B. Bryan, Bearpaw Shale: Material Properties Derived from Experiment and One-Dimensional Studies, Lawrence Livermore Laboratory, Rept. UCID-15915 (1971).
5. W. E. Baker, P. S. Westine, and F. T. Dodge, Similarity Methods in Engineering Dynamics (Haden Book Company, Rochelle Park, N. J., 1973).
6. E. L. Lee, H. C. Hornig, and J. W. Kury, Adiabatic Expansion of High Explosive Detonation Products, Lawrence Livermore Laboratory, Rept. UCRL-50422 (1968).
7. E. L. Lee, Lawrence Livermore Laboratory, private communication (1973).

Appendix A
Instrumentation

TIME OF ARRIVAL MEASUREMENTS

Much of the time of shock arrival data needed for shock velocity determinations can be obtained as a bonus from the various transducers used primarily for other measurements. The data available, however, may not be from interesting locations or there may not be enough locations to give the coverage desired. Accordingly, we added rate sticks and slifers in some locations to provide specific TOA data.

Rate Sticks

Rate sticks were used to monitor detonation velocities in several different quadrants of the spherical explosive. This data was analyzed later to determine the detonation characteristics of the explosive in shot configuration.

A rate stick (shown in Fig. A-1) is 10 piezoelectric crystal pins in a linear array. Each pin is placed at a fixed and precise location relative to an arbitrary point. When hit by the detonation wave front, these pins depolarize and give very large electromagnetic signals. If these signals are recorded as a function of time, this data can be analyzed in conjunction with the pin locations to give detonation wave times of arrival and therefore detonation velocities. Normally, the pins have brass outer conductors. However, chemical compatibility tests showed that brass corroded quickly with the HE compositions being used. Consequently, aluminum was substituted for the outer conductor pins.

Three short rate sticks and one long stick were placed in the charge cavity of each shot. Figure A-2 shows their placement and relative positions.

Slifers

Slifer systems were placed in the open hole of the 12.5-m unstemmed shot and in

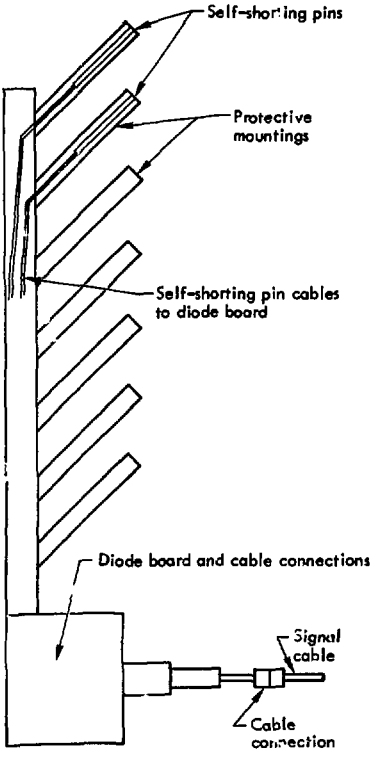

Fig. A-1. Typical rate stick construction for Phase IIA detonations.

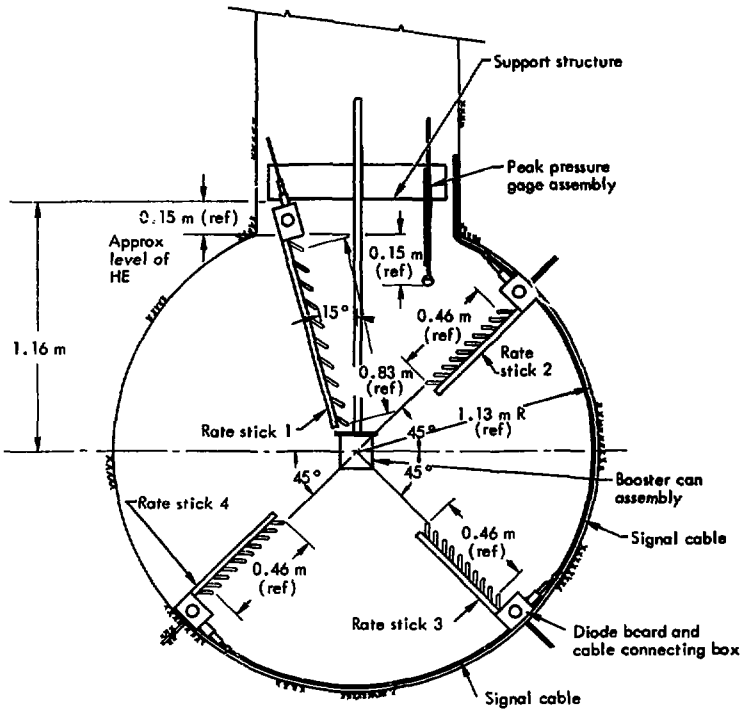

Fig. A-2. Rate stick emplacement.

he stemming of the other two shots. "Slifer" is an acronym for "Shorted Location Indication by Frequency of Electrical Resonance." The slifer system is a simple system consisting of a Colpits electronic oscillator and a long coaxial cable (see Fig. A-3). Since a shorted transmission line appears to be inductive for frequencies between zero and a frequency equivalent to a quarter wavelength, a coaxial cable operating in this domain will function as a part of the inductance in the oscillator's resonance circuit. If cable and oscillator are emplaced in a known configuration near a detonation so that the advancing shock wave crushes and shortens the resonant cable, the rate of change in the oscillator's frequency then is directly related to the shock wave velocity.

The operating frequencies of the slifer units used for these experiments were too high for direct recording on magnetic tape. The slifer's oscillatory signal was

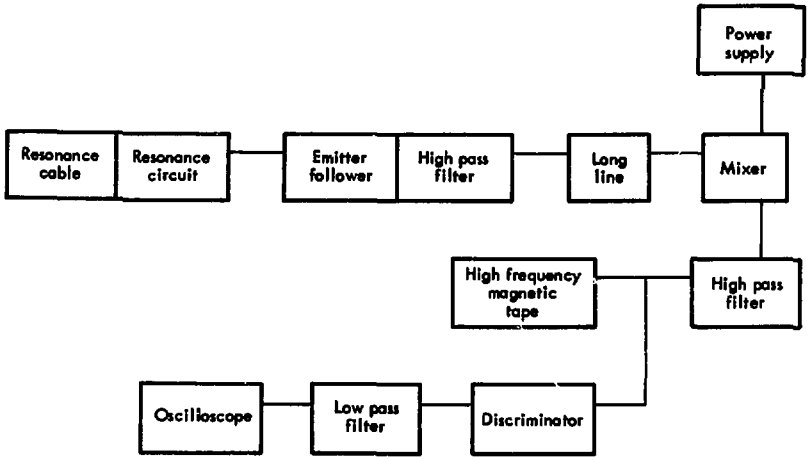

Fig. A-3. Slifer TOA system.

therefore mixed with another signal to produce a lower beat frequency so that the data could be recorded. Since the beat frequency from this mixing operation can be almost any value, depending only on the frequencies of the slifer and the local oscillator, a good match between slifer bandwidth and recorder bandwidth could be obtained.

In the field operation, the local oscillator frequency was inadvertently set too close to the slifer frequency. This proved to be disastrous because the slifer frequency moved much too close to the local oscillator frequency during the shot, causing the beat frequency to pass through zero. The low frequency response of the playback system is not low enough to process this kind of data, and about half the slifer data was lost.

PRESSURE, STRESS, AND STRAIN MEASUREMENTS

Plastic Gage

The plastic gage is a pressure transducer designed for use in the 5-25 GPa pressure range. It consists of a small spherical Lucite shell (50.8 mm in diameter), plated on the inner and outer surface to facilitate signal acquisition (see Fig. A-4). Passage of a strong shock wave through the shell wall produces preferential alignment of the polar molecules in the Lucite. This molecular alignment changes the volume polarization and thus induces a surface charge on the plated electrodes. To establish this surface charge, an electrical current must flow in some external circuit. This current is directly proportional to the amplitude of the shock wave and is the quantity recorded in this measurement.

This transducer can be used only as a peak reading instrument. Because no instruments were available that would provide analog data, we had to use this gage for a pressure measurement inside the high explosive material.

The transducers were attached to the HE filling tubing such that the sensitive surface of the transducer was ~0.15 m into the top hemisphere of the HE. This location was selected so that the gage would be far enough away from the booster charge to be unaffected by its higher pressures and far enough away from non-HE objects to be unaffected by reflected signals. Consequently, data from this gage should be a good indication of the pressure in the HE detonation front.

The electronics recording system was very simple. The gage was attached directly to the end of a RG213U coaxial cable, and data was transmitted through this cable to the recording trailer. At the recording trailer, the cable was equalized for frequencies up to 10 MHz. For recording, the cable was terminated in 50 Ω, and the signal was applied directly to the input amplifier of the recording oscilloscopes. An experimental height-to-width recording system, shown in Fig. A-5, was also used to record this data.

The low end of the frequency response curve of this gage is very high. Therefore, if the gage is to function at all, the rise time of the shock front generated by the HE detonation must be very narrow, on the order of 100 ns. In particular, no signal will be generated if the HE deflagrates rather than detonates.

HE deflagration apparently occurred in the two stemmed events since no data was recorded. Other explanations are possible: transmission line failure; incorrect assembly of the transducer; improper gage emplacement. However, they are not very likely because the system appeared to be functioning properly

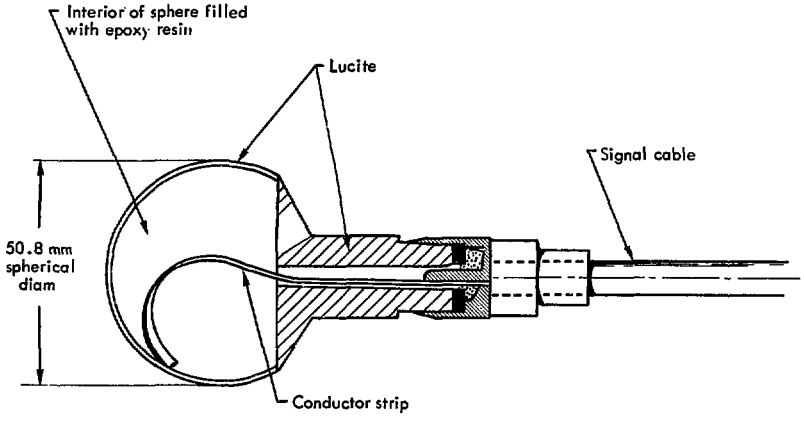

Fig. A-4. Spherical Lucite gage.

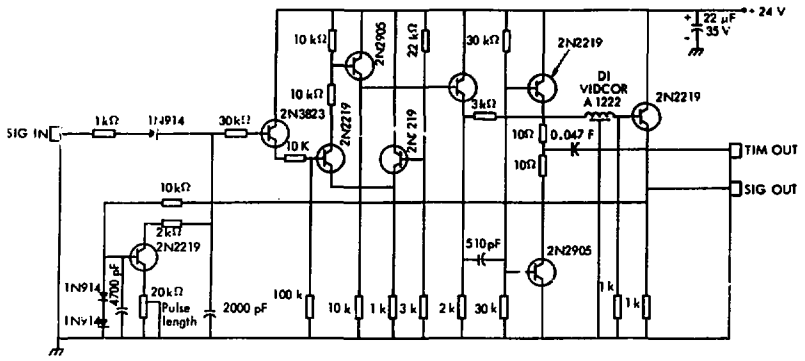

Fig. A-5. Height-to-width converter.

shortly before shot time, and all the field notes indicate that gages were emplaced properly. The absence of data from the plastic gages, combined with several other factors, leads to the conclusion that the HE in the stemmed shots failed to detonate properly.

Stress History

The stress history transducers consisted of x-cut quartz crystals with protective and connective hardware. X-cut quartz is piezoelectric; when compressed in the x-direction, it exhibits an increase in free surface charge. The transducer crystal is operated in a charge mode configuration; with the addition of a shunt capacitor, a voltage signal is produced. This signal travels through a solid dielectric coaxial cable to the ground surface where it is fed into a VCO. The VCO converts the analog signal to a frequency-modulated signal for transmission to the recording trailer and for subsequent recording on magnetic tape. Figure A-6 is an electronics schematic of this system.

Two different sets of hardware were used for the Phase IIA experiment. One set (shown in Fig. A-7a) was designed to function when the impinging shock wave travels parallel to the cable-transducer system. This design incorporates one 19.05 mm diameter, 3.175 mm thick crystal and is used either directly above the explosion for radial stress or near the shot horizon for transverse or tangential components. The other set of hardware was designed to function when the impinging shock wave strikes perpendicular to the cable-transducer system. Two identical crystals are employed in this design (shown in Fig. A-7b), which is used either directly above the detonation point for tangential measurements or at the shot horizon for radial components. Table A-1 lists gage locations and types of hardware used at each location.

Many of the stress gages did not perform over long time periods, although signals were received from the surface-mounted VCO for several hundred milliseconds. In most instances, the recorded

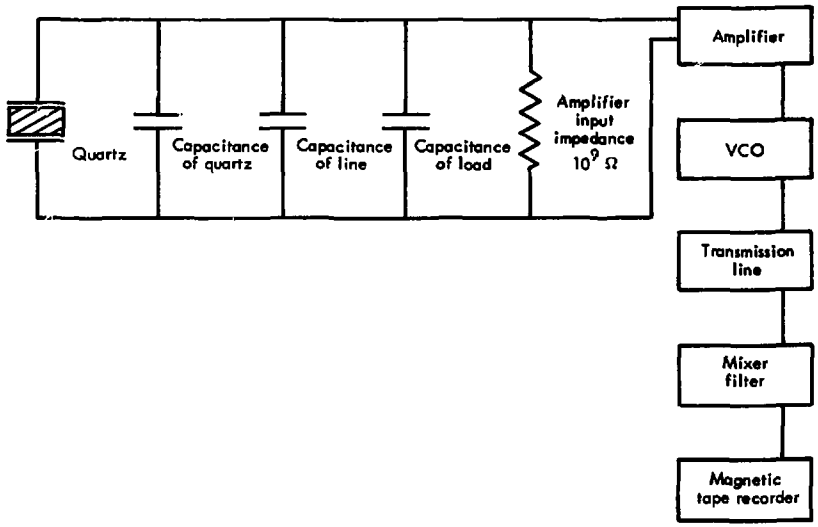

Fig. A-6. Electronics schematic for stress history transducers.

signal rose to a first peak and then flattened out or continued to rise discontinuously over several hundred milliseconds. Since the shock front should be only a very few milliseconds in duration, the signal is clearly inaccurate.

The most likely cause of failure is a break in the circuit between the crystal and the surface-mounted shunt capacitor. Normally a signal cable would be expected to fail in a shorted condition, which would immediately drive the signal output to

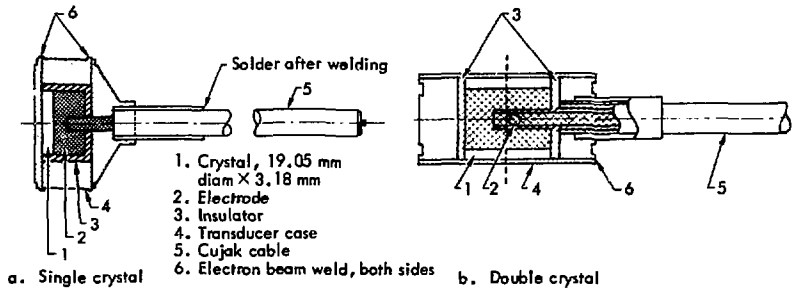

Fig. A-7. Stress history transducers.

Table A-1. Stress history instrumentation.

	Gage	Range (m)	No. of crystals	Capacitance (μF)	Arrival time (ms)	Peak amplitude MPa	Δt, signal (ms)	Δt, carrier (ms)	Comments
Unstemmed	ST-103R-A	11.58	1	0.0738	3.28	60	4.4	4.4	Good signal
	ST-107R-A	10.36	1	0.142	2.86	100	4.4	4.4	Good signal
	ST-112R-A	8.84	1	0.1158	2.43	330	4.4	4.4	Good signal
	ST-118R-A	7.01	1	0.136	1.91	450	4.4	4.4	Goes bad at onset of stress
Unstemmed	ST-D03V-A	11.36	1	0.086	NA	NA	0	17	Never functions properly
	ST-D03HR-A	11.36	2	0.152	6.4	28	100	7 100	Poor signal-to-noise ratio
	ST-D18V-A	6.86	1	0.1355	3.0	120	20	300	Goes bad at onset of stress
	ST-D18HR-A	6.86	2	0.2538	3.0	130	0	800	Goes bad at onset of stress
Unstemmed	ST-A40R-A	4.51	2	0.321	1.58	780	0	2 200	Questionable
	ST-A20R-A	7.59	1	0.1134	3.32	500	150	1 600	Good signal
Unstemmed	ST-B40R-A	15.15	2	0.1355	6.9	210	40 ?	>10 000	Good signal
	ST-B40T-A	15.15	2	0.0323	7.1	210	200	>10 000	Good signal
Unstemmed	STR-C40R-A	30.39					0		Failed
Stemmed	ST-A40R-B	4.05	2	0.305	1.48	340	70	1 480	Good signal
	ST-A20R-B	7.31	1	0.134	3.55	–		880	Questionable
Stemmed	ST-B40R-B	14.72	2	0.140	6.9	100	>500	>2 000	Good signal
	ST-B40T-B	14.72	2	0.0324	7.1	140	>500	>2 000	Good signal

zero. In this case, the opposite usually occurred, i.e., the signal increased in value.

An increase in signal can happen only if the capacitive load of the system is suddenly changed. This results only from loss of contact with some part of the system: at the least, loss of the quartz crystal; more likely, loss of the crystal plus all or some of the signal cable. This loss of capacitive load is caused by a separation in the signal line, either in the quartz crystal case or in the coaxial cable. The failure is more likely to have been inside the transducer case because it is one of the weaker links in the signal transmission system. The possibility of shorted cables cannot be completely eliminated, however; high resistance shorts for short times or low resistance shorts for very, very short times could also produce the observed results.

In future experiments, conditions leading to both kinds of failure could be changed or eliminated to give a higher probability of obtaining good data. A simple design change in the transducer case would enable it to withstand much higher pressure, and rerouting the signal cables would provide much better cable protection.

Strain

The strain transducer was built at LLL. The active element was a Pickering* linear variable differential transformer (LVDT) that was rigidly mounted to a circular steel plate (see Fig. A-8).

*Reference to a company or product name does not imply approval or recommendation of the product by the University of California or the U.S. Atomic Energy Commission to the exclusion of others that may be suitable.

Its center core was attached to a thinner plate and the ends of a brass bellows were attached and sealed to the two plates. This arrangement prevented grout and water from reaching the LVDT and also created a void space for contraction. With the LVDT monitoring the separation of the bellows, the transducer could expand or contract in response to the surrounding soil, making it sensitive to one-dimensional strain.

This particular LVDT generated analog signals and required only a dc voltage as input. The analog signal was amplified and fed to a VCO for conversion to an FM signal for transmission to the recording trailer. At the trailer the FM signal was recorded on magnetic tape.

This transducer system did not give data. The mode of failure is not evident; the only clue is a record showing the VCO frequency immediately going to band edge when the unit was hit by the shock wave. One possibility is a failure of the power or signal leads between the VCO and the LVDT. These leads did not have much protection and may have been severed by differential motion between transducer parts.

ACCELEROMETERS

All accelerometers were piezoelectric devices that were constrained to function as electric charge generators. The accelerometers, however, were not all alike in mechanical construction; units could be chosen for either of two stress configurations in the piezoelectric material. One type was a single-ended compression construction designed for compressive stress in the piezoelectric

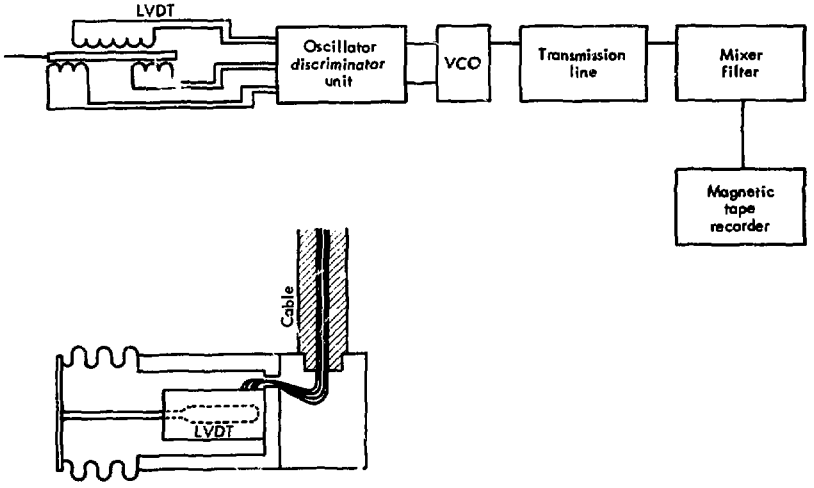

Fig. A-8. Strain gage transducer.

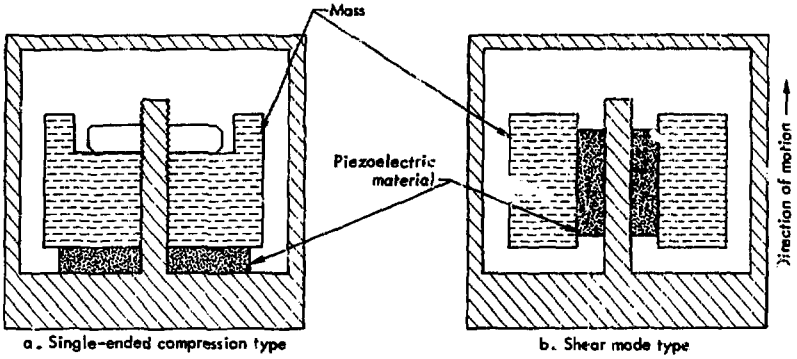

Fig. A-9. Accelerometer schematics.

material (shown in Fig. A-9a). The gages listed as model 2255 in Tables A-2 and A-3 were of this design. The other type was a shear mode construction that produced shear stresses in the peizoelectric material (see Fig. A-9b). The gages listed as model 2224 or 2225 in Table A-2 were shear mode units. Tables A-2 and A-3 list gage types and other pertinent data for accelerometers and velocity gages.

We considered several factors in choosing the type of accelerometer for any particular location. The most important ones were the peak value of the expected signal, the likelihood of a baseline shift, the sensitivities of each accelerometer unit, and the low susceptibility of shear mode accelerometers to baseline shifts. The very high signal levels predicted for some locations were expected to produce baseline shifts, especially in the compression type accelerometers. Large baseline shifts may significantly change the peak acceleration levels, and they certainly create significant problems if acceleration signals are integrated.

Shear mode accelerometers seemed the best except for their low sensitivity. Low sensitivities and low acceleration levels combine to create poor signal-to-noise ratios, which in turn produce poor data. Low signal levels, however, are not as likely to produce baseline shifts. Therefore, it was prudent to use shear mode units in the locations where high accelerations were expected and to use single-ended compression units in the locations where lower accelerations were expected.

Other factors we considered in gage selection were (1) the availability of compression units from earlier programs compared to the advisability of purchasing more shear mode units, and (2) the capability of the fielding system to respond to last-minute changes in program. After much consideration, we decided to use the already-available compression units. Shear mode units were used in the more

Table A-2. Surface accelerometers and velocity gages.

	Gage	Range (m)	Gage type	Sensitivity (limit)	Capacitance (μF) or carrier frequency (kHz)	Set recording range m/s^2	Recorded amplitude	Signal arrival (...)	Comments
12.5-m, unstemmed	Ac-S05V-A	12.59	2255	2.61 ρC/m/s^2 (98 000 m/s^2)	0.02268	4 900-78 400	39 200 m/s^2	8.34	Carrier dies at 1 s
	Ve-S25V-A	14.60		(67 m/s)	24.8		53 m/s	12.5	Both carriers die at 2 s (thermistor)
	Ac-S50HR-A	18.75	2224	1.12 ρC/m/s^2	0.0016	980-14 700	392 m/s^2	18.1	Poor signal-to-noise ratio. Carrier dies at 2 s.
	Ve-S50V-A			(9800 m/s^2)	24.7		15 m/s	18.0	High carrier dies at 2 s. Low carrier goes away at 30 ms
	Ac-S80V-A	27.34	2224	1.11 ρC/m/s^2 (9800 m/s^2)		294-4 900	617 m/s^2	27.1	>2 s
	Ac-S80HR-A		2255	2.39 ρC/m/s^2 (98 000 m/s^2)	0.00204		235 m/s^2	28.9	>5 s
12.5-m, stemmed	Ac-S05V-B	12.62	2255	2.53 ρC/m/s^2 (98 000 m/s^2)		4 900-78 400	29 400 m/s^2	8.3	Carrier dies at 750 ms
	Ve-S25V-B	14.5		(67 m/s)					1-MHz carrier starts at 400 ms with subcarrier (thermistor)
	Ac-S50HR-B Ve-S50V-B	18.41	2224	11.5 ρC/m/s^2 (9800 m/s^2)	0.00173	980-14 700	980 m/s^2	17.6	>1 s carrier subcarrier dies at >1 s carrier
	Ac-S80V-B	26.97	2255	2.40 ρC/m/s^2	0.00205	294-4 900	1 080 m/s^2	22.9	>2 s
	Ac-S80HR-B		2255	2.40 ρC/m/s^2 (98 000 m/s^2)	0.00205		206 m/s^2	23.1	>2 s
6-m, stemmed	Ac-S05V-C	6.22	2225	0.075 ρC/m/s^2 (186 000 m/s^2)	0.001092	7 840-98 000	117 600 m/s^2	3.20	30 ms carrier
	Ac-S20V-C	9.69	2255	2.61 ρC/m/s^2 (98 000 m/s^2)	0.02318	4 900-78 400	24 500 m/s^2	5.6	Double VCO 700 ms carrier
	Ve-S40V-C	14.97		(61 m/s)					2 s 1 MHz carrier (thermistor)
	Ve-S40HR-C			(61 m/s)					2 s of carrier and subcarrier
	Ac-S65V-C	20.66	2224	0.99 ρC/m/s^2 (9800 m/s^2)	0.00182	980-14 700	735 m/s^2	25.0	>5 s of carrier
	Ac-S65HR-C		2224	1.15 ρC/m/s^2	0.00172	980-14 700	294 m/s^2	25.7	2 s of carrier

crucial locations, with the compression units used for the remainder of the accelerometer stations in the program.

The electronics system was the same as that used for stress history measurements.

Three major problems plagued the analysis of the acceleration data: hardware failure, baseline shifts, and poor signal-to-noise ratios. The hardware failures were similar to the hardware failures encountered in the velocity measurements, described in the following section on particle velocity measurements.

Baseline shifts were the biggest problem encountered when using integrated accelerometers for velocity gages, particularly for high peak accelerations with short durations. Moreover, it was difficult to locate the baseline shifts because most were down in the noise and were therefore not immediately obvious.

Electronic discrimination problems that give results similar to baseline shifts are produced by a limitation in recording level. An electronics system set to record signals of 98 000 m/s^2 peak levels cannot accurately measure the low

Table A-3. Shot-level accelerometers and velocity gages.

	Gage	Range (m)	Gage type	Sensitivity (limit)	Capacitance (μF) or carrier frequency (kHz)	Set recording range m/s^2	Recorded amplitude (m/s^2)	Signal arrival (ms)	Comments
Unstemmed	Ac-A40R-A	4.51	2225	0.075 $\rho C/m/s^2$ (196,000 m/s^2)	0.00202	7840-98000	196,000	1.64	Carrier 1.7 s 1.75 ms to cable break
	Ve-B40R-A	15.15	Highly over-damped	36.5 m/s					(Thermistor)
	Ve-B40T-A			12.2 m/s	55 kHz		No signal	7.5	No signal: low frequency Carrier dies when hit High frequency carrier okay
	Ac-C40V-A	30.39	2224	1.11 $\rho C/m/s^2$ (9800 m/s^2)				14.6	Failed during fabrication (thermistor)
	Ve-C40R-A			(12.2 m/s)	40 kHz	98-1470	No signal		A bit of low frequency carrier that dies when hit. High frequency carrier okay
Stemmed	Ac-A40R-B	4.05	2225	0.074 $\rho C/m/s^2$ (196,000 m/s^2)	0.00199	7840-98000	≈98,000	1.88	Carrier to 1.7 s 2 ms to cable break
	Ac-B40V-B	14.72	2224	1.15 $\rho C/m/s^2$ (98,000 m/s^2)	0.00208	490-7840	No signal	7.0	Carrier longer than 5 s (thermistor)
	Ve-B40R-B			36.5 m/s			No signal	7.1	No signal: low frequency Carrier dies when hit High-frequency carrier dies shortly thereafter.
	Ac-C40V-B	29.96	2255	2.30 $\rho C/m/s^2$	0.00340	98-1470	No signal	14.5	More than 2 s of carrier. (thermistor)
	Ve-C40R-B			(12.2 m/s)					Higher carrier stops at 100 ms

level negative accelerations needed to bring the velocity signal back to zero.

The accuracies of the peak acceleration determinations are limited to about ±25%. Accuracy is limited for the high frequency components by the filtering used in the playback system and for the low frequency components by the signal-to-noise ratio. Neither of these problems is as critical for accuracy as the baseline shifts, however. The baseline shifts make it difficult to assign accuracies to integrated velocities.

PARTICLE VELOCITY MEASUREMENTS

The particle velocity transducer used for these measurements was a highly damped mass-spring mechanical system, shown in Fig. A-10. The gage was developed by the Stanford Research Institute,[A-1] with some later improvements by Sandia Laboratories, Albuquerque.[A-2] The gage has proved to be useful in many areas and has been extensively used.

The system consists of a pendulum (mass) and a volume of viscous silicone oil. The pendulum is actually a padule that is placed in the liquid such that its motion is constrained only by its pivots and the viscosity of the liquid. If the frequency content of the input signal is limited to a small frequency span centered about the resonance frequency of the paddle system, then the angular displacement of the paddle is proportional to the magnitude of the velocity imparted to

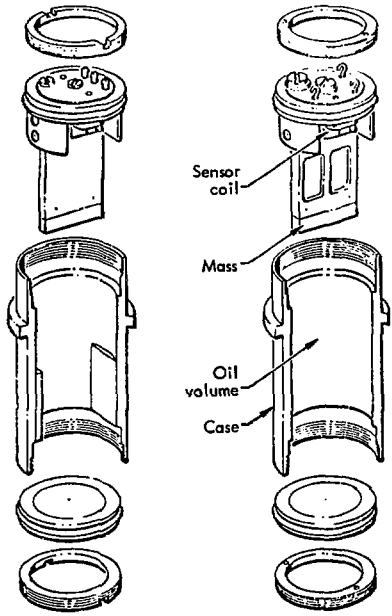

Fig. A-10. Particle velocity gage.

the transducer case. Given these operational conditions, the system will measure the particle velocity of the surrounding rock as long as transducer case is well coupled to the rock.

A variable reluctance system is used to sense the angular displacement of the paddle. Two coils are rigidly mounted to the case so that the ends of the coils are close to two blades attached to the free moving paddle. As the paddle moves, the spatial separation between coil and blade changes. Since the inductances of the two coils directly depend on the separation between coils and blades, any change in paddle position is reflected by a change in inductances of the two coils. These two inductances are used to control the frequencies of two local oscillators, and the paddle position can be determined from the relationship between the frequencies of the two oscillators. The outputs of the two oscillators are beat together to reduce the number of signal channels and to reduce the dependence of the paddle position measurement to just one frequency. Using the appropriate calibrations, this output frequency can be made directly proportional to the velocity experienced by the transducer case. Figure A-11 is a schematic of the velocity gage and the associated electronics.

The beat frequency or subcarrier (low frequency carrier) is immediately passed through a bandpass filter. This filter was not necessary for this application but was used because it was part of an available package. In this system several signals were multiplexed to the same transmission line, and the bandpass filter was used to prevent one particular signal from deviating into another signal's frequency band.

After passing through the bandpass filter, the signal was used to modulate a VCO with a center carrier near 1 MHz. Again, this conversion was not necessary, but this VCO unit contained a power voltage source for the low frequency oscillators. Otherwise an extra cable for power would be needed for each gage, adding substantially to the cost. The 1-MHz FM signal was carried to the recording trailer via R6213U coaxial cable and recorded directly on magnetic tape.

Velocity gage performance was extremely poor. Of the 11 systems

emplaced (see Tables A-2 and A-3), only one gave a signal of any value. The gages can be classified by performance characteristics as follows:

Good Signal
- Ve-S25V-A

Dead at shot time
- Ve-B40R-A
- Ve-C40R-B
- Ve-S25V-B
- Ve-S40V-C

Operating but signal not believable
- Ve-S50V-B
- Ve-S40V-C

Operating at shot time but failed during shot
- Ve-B40T-A
- Ve-C40R-A
- Ve-S50V-A
- Ve-B40R-B

For the gages whose subcarriers stopped oscillating some time before the shot was detonated, failure took the form of slow decreases in subcarrier signal amplitudes over a period of several days. A few days after grouting, the output signal started to fail and continued to decrease until it was below the level needed to modulate the main carrier. After that time, no detectable signal was ever observed; although the probability of obtaining data was zero, the main carrier was recorded during the detonations. As expected, no data was obtained.

Since the cause of this decreasing amplitude is not known, several possible explanations need investigation.

- A subcarrier frequency shift. This explanation supposes a large deviation in the subcarrier oscillator frequency. Regardless of the cause, the frequency may have shifted beyond the limits of the bandpass filter, causing drastic signal attenuation. At first, there would have been little attenuation as the frequency

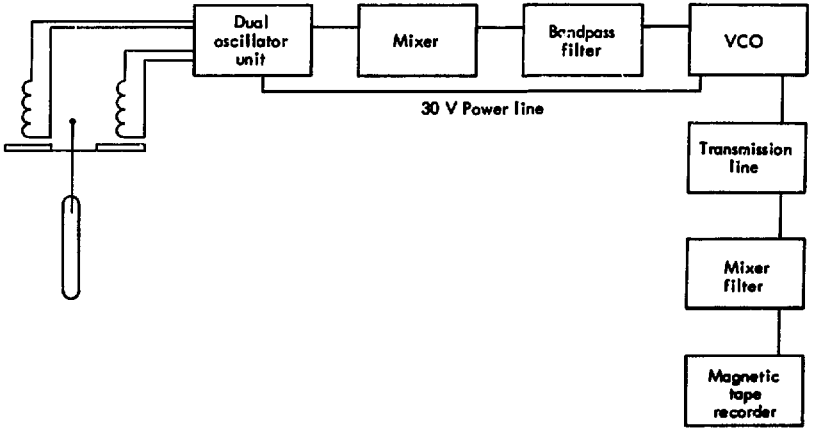

Fig. A-11. Velocity gage schematic and electronics.

approached the band edge of the filter. However, as the frequency moved through the band edge, it would have been attenuated until it finally disappeared. This may not be the correct explanation, however, because the units suffering a decrease in amplitude but still functioning at shot time had not shifted in frequency. Unfortunately, the dead ones were not monitored during their demise.

- A water leak. Water leaks were possible, and the likely entry was through the thermistor ports. Thermistors were needed to monitor the temperature of the oil at shot time, since the viscosity of the oil, an integral parameter in deriving the gage sensitivity, was determined by the temperature.

A water leak could have caused either or both of the following situations. First, the conductivity of the water could have slowly driven any or all of the electronic circuits to ground. Second, the presence of water in the local oscillator's tank circuit could have caused the frequency of that oscillator to deviate drastically. Either of these situations might have given the results observed.

- An electronic component failure.
- An electronic grounding problem.

The number of individual units in this system created a potential grounding problem. With so many electronic interfaces between the recording trailer and the velocity gage, proving the existence of grounding problems was impossible.

For the gages that failed during the shot, the canister, associated hardware, and signal transmission system were not able to survive the passage of the shock wave. This was a particular problem with the subsurface instruments. It would not have been difficult to make these gage systems hard enough to survive in most of the gage locations. This kind of hardware, however, would not have been compatible with making good stress history measurements. Since a stress history measurement was the primary goal, it was not possible to give the velocity gages the protection normally given. Hindsight suggests that it would have been much better to separate the two measurements into different packages and into different holes, but cost and time factors were prohibitive.

Two gages experienced an unexplained mode of failure. These units appeared to be functioning properly, but their outputs did not resemble anything that might be construed as a proper signal. They may have been assembled incorrectly.

TELEMETRY AND RECORDING

All data was transmitted over coaxial cable to the recording trailer, located 1000 feet away. All data was transmitted as 1 MHz FM signals except for the plastic gage and rate sticks, which were transmitted as analog signals. For transmission, analog signals were converted to FM signals with VCOs. These oscillators and their signal transmission cables were rigidly fastened to the surface concrete pads. After leaving the pads, the cables were spread out across the ground so as to provide enough excess cable to spread over the rising mound during cratering. Cables for subsurface VCOs and analog signals were similarly spread on the ground. Cabling was somewhat different for these units in that a large vertical loop of cable was used at the

hole exit. These precautions were very effective and little data were lost because of land line failure.

Generally, data recording was on magnetic tape with wide bandpass oscilloscopes as a backup system. Because of the high frequency range required by the plastic gage and the rate sticks, they were recorded on oscilloscopes only.

APPENDIX A REFERENCES

A-1. L. M. Swift, Development of an Earth Velocity Gage, Defense Atomic Support Agency, Washington, D.C., Rept. DASA-1191 (1960).

A-2. W. P. Perret, J. W. Wistor, G. J. Hansen, and D. G. Palmer, Four Papers Concerning Recent Work on Ground Motion Measurements, Sandia Laboratories, Albuquerque, N. M., Rept. SC-R-65-904 (1965).

Appendix B
Emplacement Procedure

The emplacement plan consisted of placing transducers in vertical holes and in surface pads. All transducers for each station were placed in a single 0.15 m diam canister. The length of the canister varied with the kinds of transducers used. Figures B-1 and B-2 give some examples. After the instruments were in the canisters and were oriented in the proper direction, the canisters were filled with a DF-5 grout mixture.* The assembly and pregrouting were done at LLL before shipment to the field.

For subsurface emplacement, the grouted transducer canisters were placed in a downhole string made up of the canisters and appropriate lengths of 76 mm diam polyvinylchloride pipe. This

*DF-5 Grout Formula:

Type G cement	15.06 kg
Gel Bentonite	1.81 kg
Barite ($BaSO_4$)	12.02 kg
Monterey Sand (20-40)	12.79 kg
CFR-2 (friction reducer)	0.059 kg
Air entraining agent (NVX Powder or Vinsol Resin)	0.397 kg
Water	15.06 kg

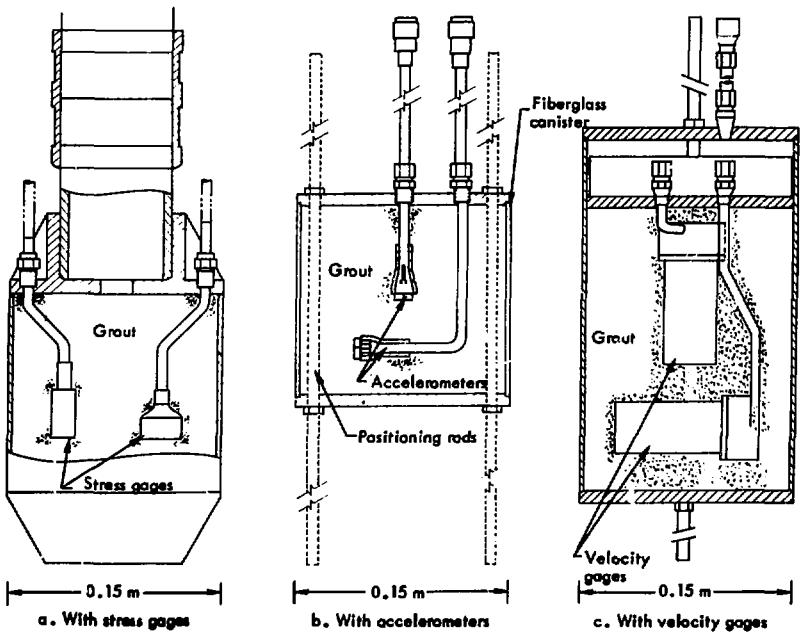

Fig. B-1. Examples of pregrouted transducer canisters.

string was assembled horizontally on the ground surface and checked electronically before insertion into the instrument hole. A nylon rope was fastened to the top of the instrument string and looped around a piece of rod near the top of the drill rig. Using this support, the downhole string was lifted into a vertical position. The string was then lowered into the instrument hole, which was nominally 304.8 mm in. in diameter and 13.7 m deep. After emplacement, the string was oriented manually to obtain the proper alignment for radial and tangential measurements. Immediately after orientation, the hole was backfilled with the DF-5 grout mixture.

For the subsurface instrumentation, the electronics conditioning systems were placed on separate surface pads. The exception was the velocity gages, whose electronics conditioning systems were located in the instrument hole, near the transducers.

For surface installation, the canisters were placed just below the surface in an excavated volume 0.91 m by 1.22 m and 0.46 m deep. After positioning and orientation, the open volume was filled with ready-mix concrete (see Fig. B-3). The associated electronics conditioning systems were placed on the same pad.

Three LLL trailers were taken to the site for field operations. One, a mechanical trailer, was used for field checkout of the grouted canisters and for assembly of the downhole instrument strings. The second was used for data recording, and the third was a power supply for the other two trailers. Field operations, including field checkout of transducers, assembly

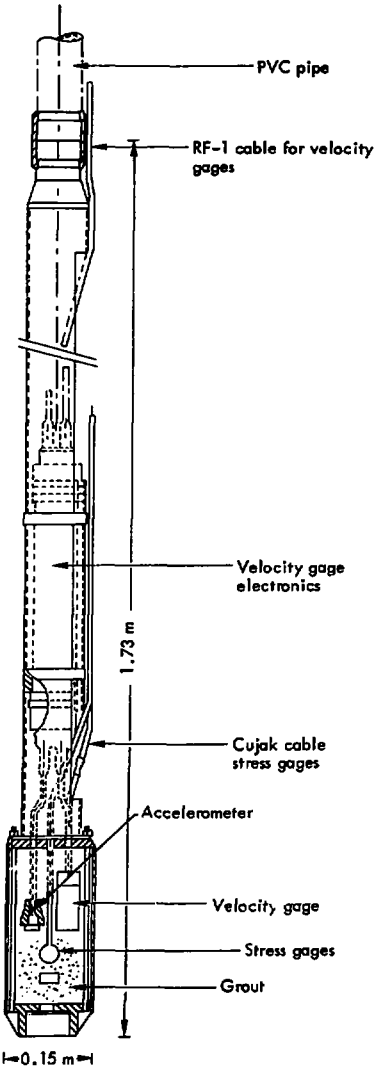

Fig. B-2. Pregrouted transducer canister with several types of transducers.

of downhole strings, emplacement of instruments, and preparation of the recording gear were accomplished during the 35 days preceding the first shot.

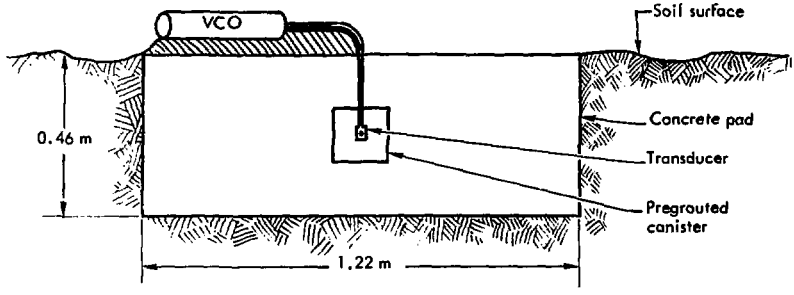

Fig. B-3. Emplacement of surface canisters.

Appendix C
Experimental Data

UNSTEMMED 12.5 m SHOT

The instrumentation plan is shown in Fig. 1. Instrument Hole A was parallel to and 4.51 m from the HE emplacement hole; instrument stations were placed 6.49 m and 12.56 m below the surface. Instrument Hole B was located 15.15 m from the HE emplacement hole. It contained one instrument station at the bottom, 12.56 m below the ground surface. Instrument Hole C, located 30.39 m from the HE emplacement hole, had one transducer station at the bottom of the hole. Instrument Hole D was parallel to the open emplacement hole and 1.4 m away. Two measurement stations (at 7.16 m and 11.67 m from the shock point) were instrumented, with each station having one single crystal transducer unit looking at the stress component parallel to the open hole and one double crystal transducer unit sensitive to the stress component perpendicular to the axis of the open hole.

The emplacement hole instrumentation included the rate sticks, one slifer, one plastic gage, and four stress history gages. The slifer extended from near the center of the HE, through the top HE hemisphere, and up the open hole to the surface. The stress history gage locations were 7.01, 8.84, 10.36, and 11.58 m from the detonation center.

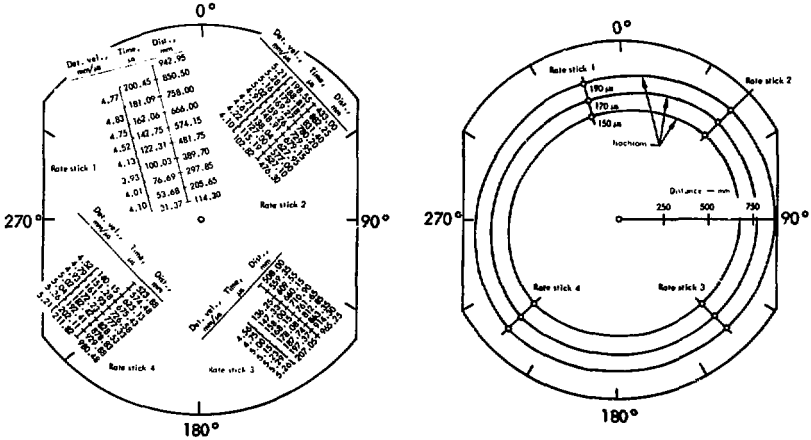

a. Detonation velocity and uniformity

b. Detonation symmetry

Fig. C-1. HE detonation history, DOIIA-1, 12.5 m, unstemmed.

There were four surface motion stations, located at 1.58, 7.56, 13.96, and 24.32 m from surface ground zero.

Figure C-1 shows the detonation history of the explosive. Figures C-2 and C-3 give the data from Hole A. Figures C-4 and C-5 give the data from Hole B. No data was received from the two velocity gages in Hole B. The subcarrier oscillator of one gage had stopped before shot time. Both oscillators for the other gage were functioning properly before the shock wave hit the transducer. At that time, both oscillators died.

All the transducers in Hole C gave no data. The velocity gage died when hit by the shock wave. The strain gage failed for some reason not yet specified, and the accelerometer failed because of a water leak during the pregrouting stage.

Figures C-6 and C-7 show the data for Hole D. Note that the stress history data in Fig. C-7b was unsatisfactory. Although this unit experienced some intermittent difficulties before the detonation, it appeared to be functioning correctly when checked just before shot time. Apparently the transducer failed even though the system as a whole appeared to be operating correctly most of the time. Another possible cause of failure is damage to the VCO by material thrown from the open hole. This could have disabled the VCO before the shock wave reached the transducer location. Regardless of the cause of failure, the negative signal received from the transducer cannot be valid, because a negative signal indicates tension in the crystal and tension is impossible in this hardware design.

Figure C-8 gives the stress history data from the open hole. Four single crystal transducer systems were placed at locations 7.01, 8.84, 10.36, and 11.58 m above the detonation center. They were placed in a jig that held them ~0.15 m from the wall of the hole and spaced them equally 90° from each other around the hole.

Since pressures were expected to be 100 MPa above the survival pressure for cables, the signal cables were protected with a 12 mm lead covering over a length extending from the transducer location to

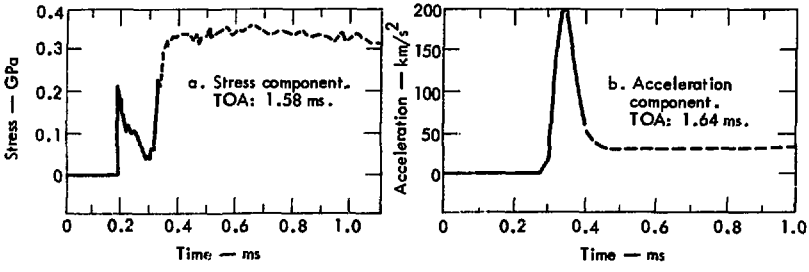

Fig. C-2. Data from A40R-A station. Horizontal range: 4.51 m; instrument range: 4.51 m; stress and acceleration components: radial. Stress data was satisfactory for 0.15 ms after onset of signal; unit failed at that time. Acceleration data over-ranged; failed at ~0.4 ms. See Fig. B-1a.

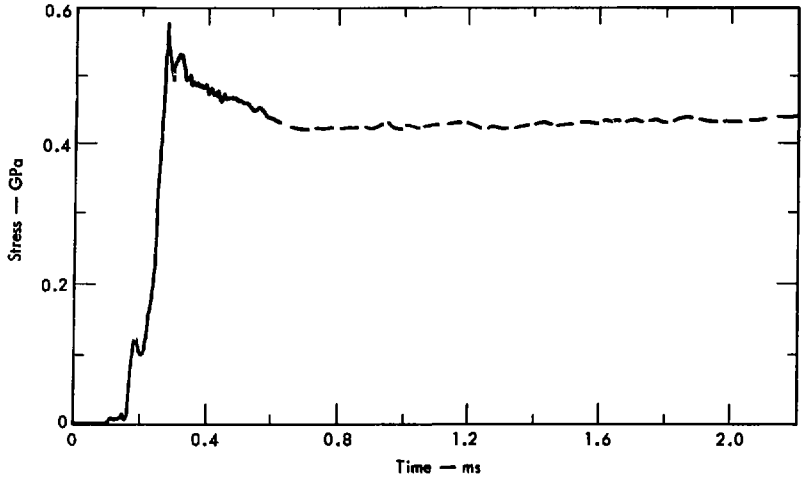

Fig. C-3. Stress history data from ST-A20R-A station. Horizontal range: 4.51 m; instrument range: 7.59 m; TOA: 3.32 ms; stress component: radial; data: satisfactory for 0.5 ms after onset of signal; failure occurred at th_* time. See Fig. B-1a.

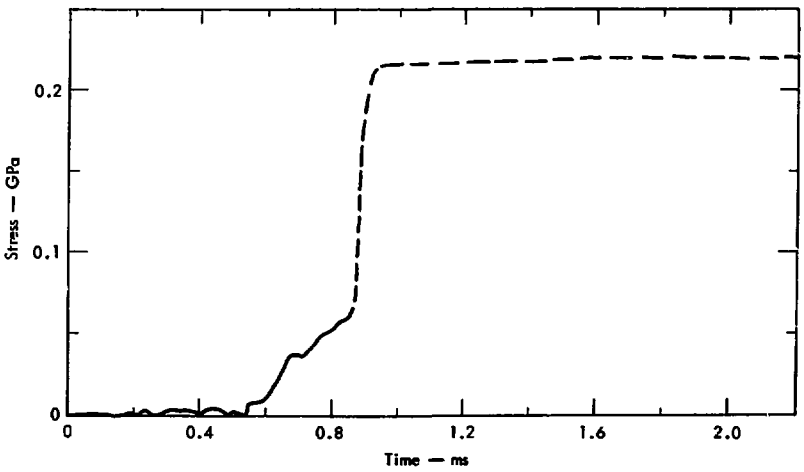

Fig. C-4. Stress history data from ST-B40R-A station. Horizontal range: 15.15 m; instrument range: 15.15 m; TOA: 6.95 ms; stress component: radial; data: satisfactory to dashed portion. See Fig. B-2.

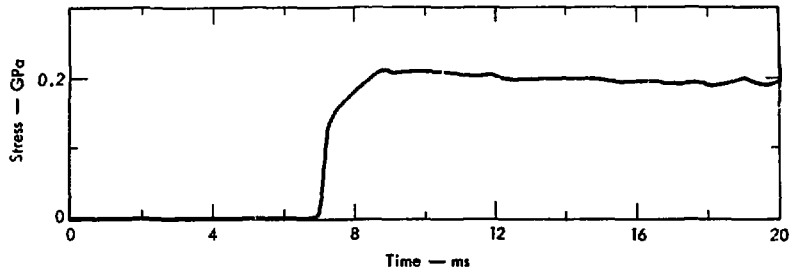

Fig. C-5. Stress history data for ST-B40T-A station. Horizontal range: 15.15 m; instrument range: 15.15 m; TOA: 7.09 ms; stress component: tangential; data: satisfactory. See Fig. B-2.

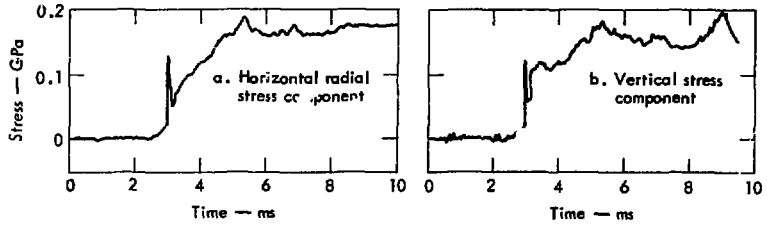

Fig. C-6. Stress history data from ST-D18HR-A and ST-D18V-A stations. Horizontal range: 1.5 m; instrument range: 6.86 m; TOA: 3.0 ms; data: satisfactory. See Fig. B-1a.

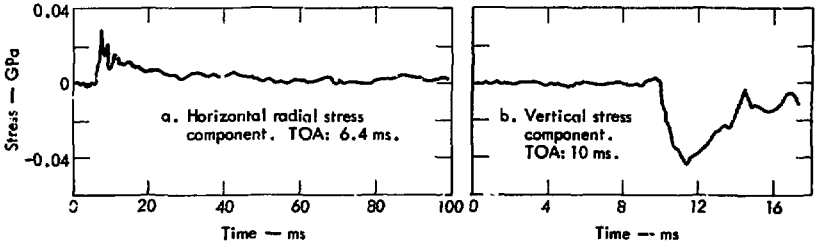

Fig. C-7. Stress history data from ST-D03HR-A and ST-D03V-A stations. Horizontal range: 1.5 m; instrument range: 11.36 m. Horizontal radial stress data was satisfactory; vertical stress data was no good. See Fig. B-1a.

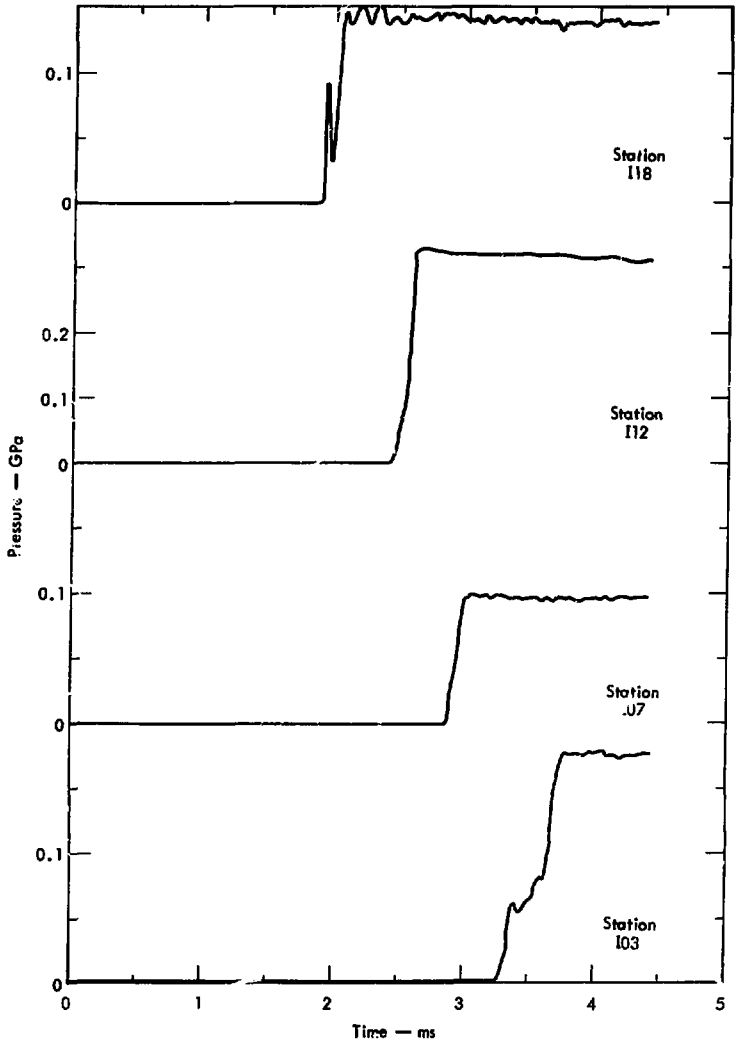

Fig. C-8. Stress history data from the open hole.

a point slightly above the ground surface.

The individual stress history systems functioned as follows:

1. ST-I18R-A, located 7.01 m above the detonation center, failed before the pressure reached its peak value. A time extrapolation gave 0.45 GPa for the peak stress amplitude. This extrapolation was done by translating the amplitude of the signal vertically and horizontally until the discontinuity was removed and the slopes matched. A signal continuous in time is the result.

2. ST-I12R-A, located 8.84 m above the detonation center, gave good data with a peak amplitude of 0.33 MPa.

3. ST-I07R-A, located 10.36 m above the detonation center, appears to give good data, although this data is not consistent with data from ST-I03R-A.

4. ST-I03R-A, located 11.58 m above the detonation center, also appears to give good data; however, the peak amplitude of this signal is larger than the peak amplitude for ST-I07R-A. Several explanations are possible, none of which can be confirmed.

First, both signals are correct. If so, it would be very hard to postulate a physical system that would give this reversal in peak amplitudes. A reflection from the surface might create such a condition, but there is not sufficient time for a reflection to return to the ST-I03R-A location. Therefore, we conclude that both signals cannot be correct.

Second, signal cables have been interchanged. This cannot be the correct explanation because the time order is correct as the signals now stand.

Third, failure occurred in the electronics systems. This is doubtful since the carrier signals on the magnetic tape record look very good, and all the related equipment appears to have been functioning properly.

Fourth, an error was made in the amplitude calibrations or in the playback conversions. Since a factor of 2 correction in either signal would be acceptable and since factors of 2 errors are easy to

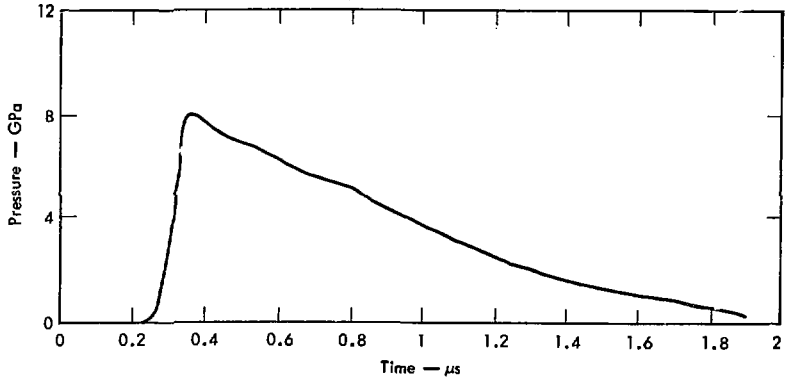

Fig. C-9. Plastic gage data from the ST-I40R-A station.

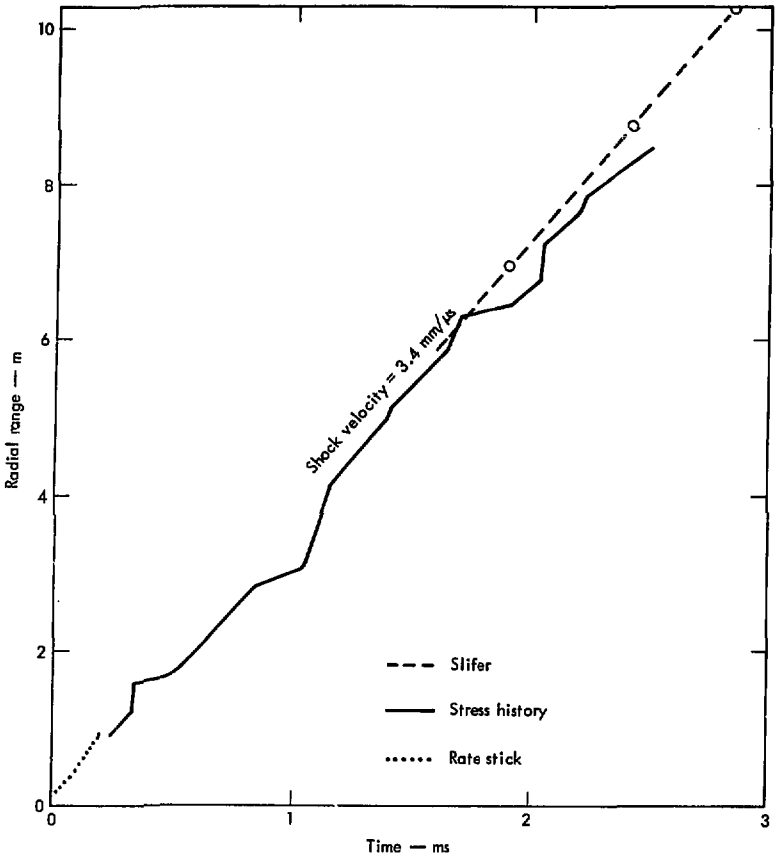

Fig. C-10. TOA data from the open hole.

make, a calibration error is the most likely explanation. There is an additional suspicion associated with ST-107R-A station. The VCO for this transducer failed before the shot and had to be replaced under less than ideal conditions, so an error was possible, especially in the measurement of the load capacitor. This measurement should not be wrong by a factor of 2, however. In addition, the measurement coincided with a previously measured value for that VCO, and there were no spare VCOs with a load capacitor of twice that value. To verify the

play-back conversions, both data channels were played back and analyzed three times with identical results.

Fifth, the ST-I07-A signal is correct, and the peak stress for ST-I03-A corresponds to the first peak of 0.06 GPa at 3.4 ms. All subsequent signal is specious, for unknown reasons. This is the only interpretation that correctly orders the amplitudes of the emplacement hole stations and is the one we accept.

Figures C-9 and C-10 give the plastic gage and TOA data, respectively.

Figures C-11 through C-16 give the acceleration and velocity data for the surface stations.

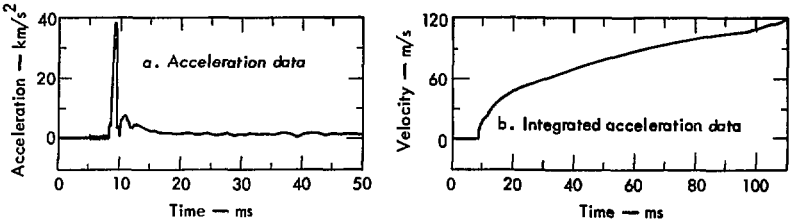

Fig. C-11. Acceleration and integrated acceleration data from the Ac-S05V-A station. Horizontal range: 1.5 m; instrument range: 12.59 m; TOA: 8.34 ms; acceleration and velocity components: vertical. Acceleration data was satisfactory. However, a baseline shift in the acceleration signal quickly drove the integrated signal into the unbelievable range. If we disregard the signal beyond 17.5 ms, we obtain a peak velocity of ~50 m/s. See Fig. B-1b.

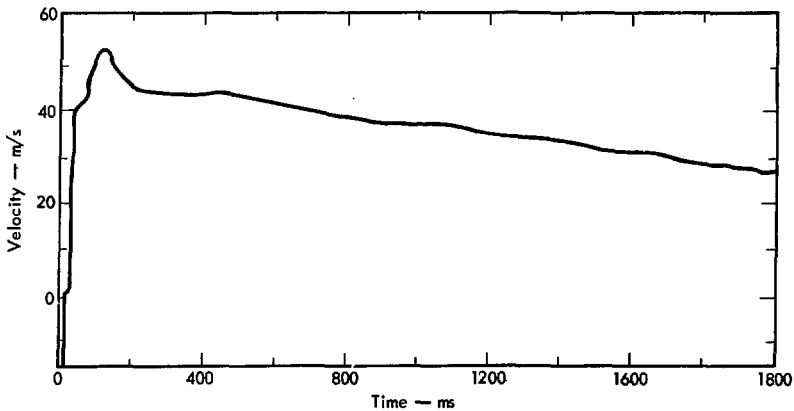

Fig. C-12. Velocity data for the Ve-S25V-A station. Horizontal range: 7.56 m; instrument range: 14.6 m; TOA: 13.0 ms; velocity component: vertical; data: satisfactory. This gage suffered a momentary failure during the signal risetime (acceleration levels were high at this location), but the remainder of the signal is satisfactory. See Fig. B-1c.

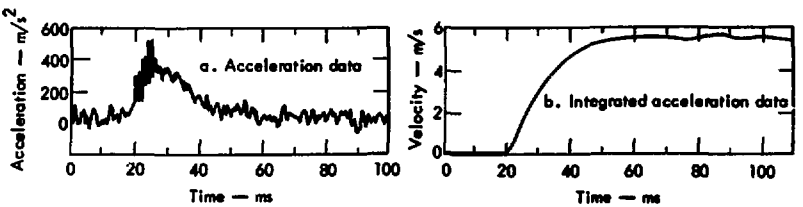

Fig. C-13. Acceleration and integrated acceleration data for the Ac-S50HR-A station. Horizontal range: 13.96 m; instrument range: 18.75 m; TOA: 18.1 ms; acceleration and velocity components: horizontal radial; data: satisfactory despite poor signal-to-noise ratio in acceleration data. See Fig. B-1b.

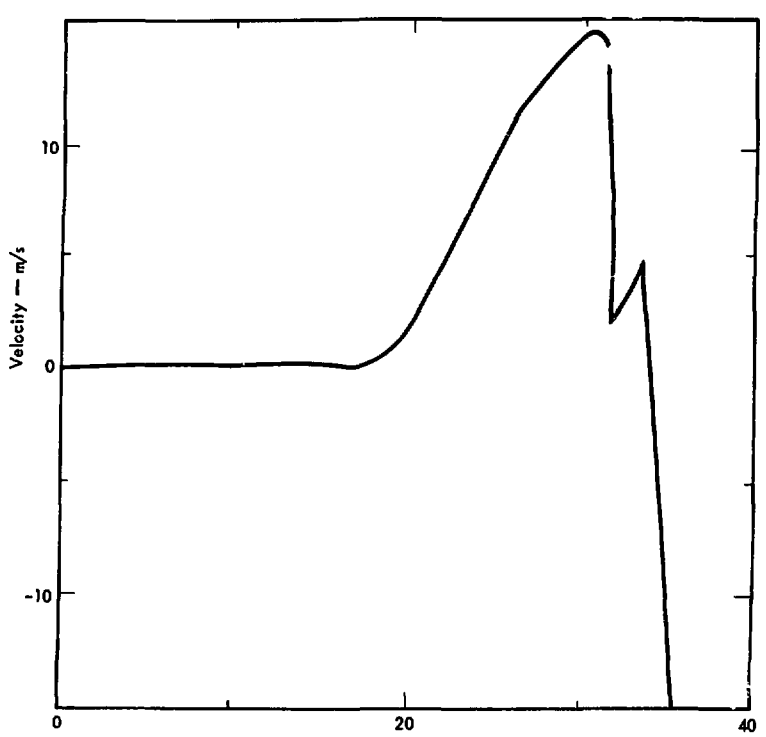

Fig. C-14. Velocity data for the Ve-S50V-A station. Horizontal range: 13.96 m; instrument range: 18.75 m; TOA: 18.0 ms; velocity component: vertical. This system failed very early, possibly before the surface reached its maximum velocity. See Fig. B-1c.

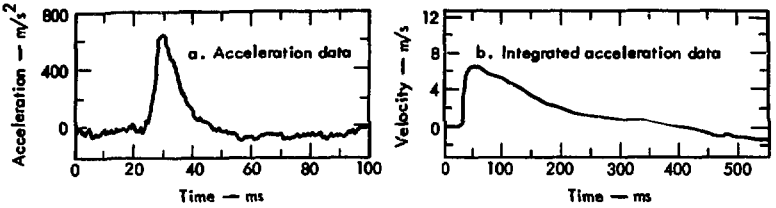

Fig. C-15. Acceleration and integrated acceleration data for the Ac-S80V-A station. Horizontal range: 24.32 m; instrument range: 27.34 m; TOA: 27.1 ms; acceleration and velocity components: vertical; data: satisfactory. See Fig. B-1b.

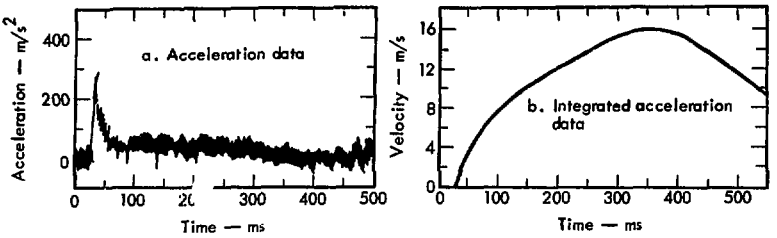

Fig. C-16. Acceleration and integrated acceleration data for the Ac-S80HR-A station. Horizontal range: 24.32 m; instrument range: 27.34 m; TOA: 28.9 ms (noise problem); acceleration and velocity components: horizontal radial. Acceleration data was satisfactory although signal-to-noise ratio was very bad. The longtime low-level acceleration caused the integrated signal to reach a large value. This value may be valid, but its size combined with the poor signal-to-noise ratio make it doubtful. See Fig. B-1b.

STEMMED 12.5 m SHOT

All the instrumentation, except for that in the HE cavity, is shown in Fig. 2. Instrument Hole A was 4.05 m from the HE emplacement hole; instrument stations were placed at depths of 6.49 and 12.59 m. Instrument Hole B was located 14.72 m from the HE emplacement hole. It contained one instrument station at the bottom, at 12.59 m. Instrument Hole C was located 29.96 m from the HE emplacement hole and had one instrument station placed at the bottom of the hole.

The emplacement hole instrumentation included the rate sticks, one plastic gage, and one slifer. The slifer extended from near the center of the HE sphere, through the top HE hemisphere, and up through the grout in the emplacement hole to the surface.

There were four surface motion stations, located at 1.68, 7.44, 13.53, and 23.9 m from surface ground zero.

Figure C-17 shows the detonation history of the explosive. Figures C-18 and C-19 give the data from Hole A. Figures C-20 and C-21 give data from Hole B. No data was received from the velocity gage in Hole B. Both oscillators were functioning properly before being hit by the shock wave. The subcarrier died immediately, and the main carrier died ~30 ms later, both as a result of signal cable breakage. The accelerometer at Ac-B40R-B station also gave no data. It failed when hit by the shock wave.

We received no data at all from Hole C. The subcarrier oscillator of the velocity gage stopped oscillation before shot time,

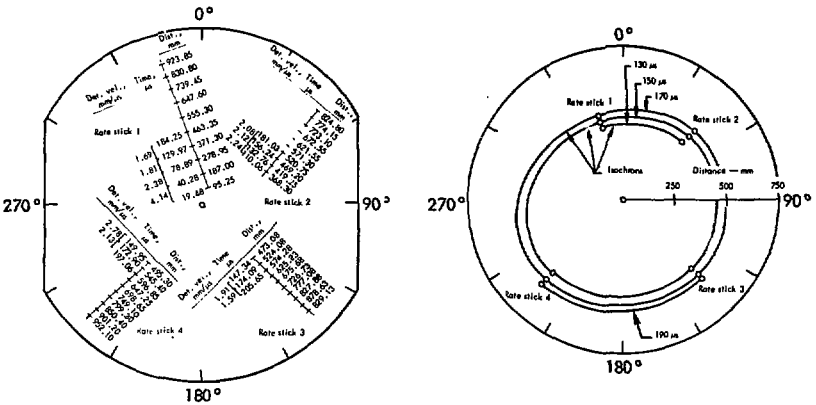

a. Detonation velocity and uniformity

b. Detonation symmetry

Fig. C-17. HE detonation history, DOIIA-2, 12.5 m, stemmed.

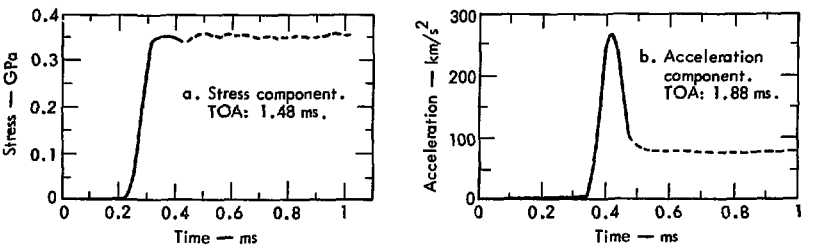

Fig. C-18. Data from A40R-B station. Horizontal range: 4.51 m; instrument range: 4.51m; stress and acceleration components: radial. Stress data was satisfactory, at least through the first peak. Acceleration data was over-ranged. See Fig. B-1a.

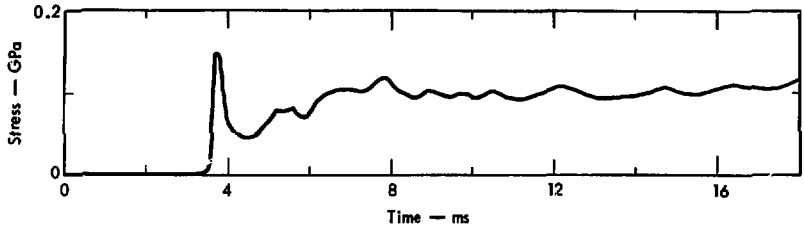

Fig. C-19. Stress history data from ST-A20R-B station. Horizontal range: 4.51 m; instrument range: 7.31 m; TOA: 3.55 ms; stress component: radial; data: questionable. See Fig. B-1a.

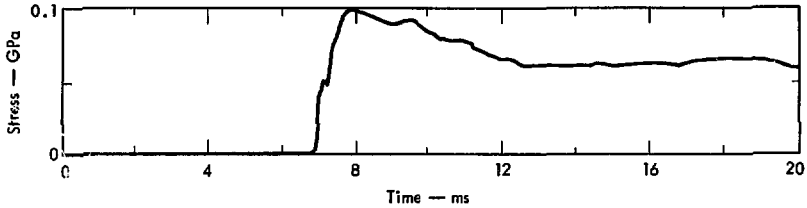

Fig. C-20. Stress history data from ST-B40R-B station. Horizontal range: 14.72 m; instrument range: 14.72 m; TOA: 6.86 ms; stress component: radial; data: satisfactory. See Fig. B-2.

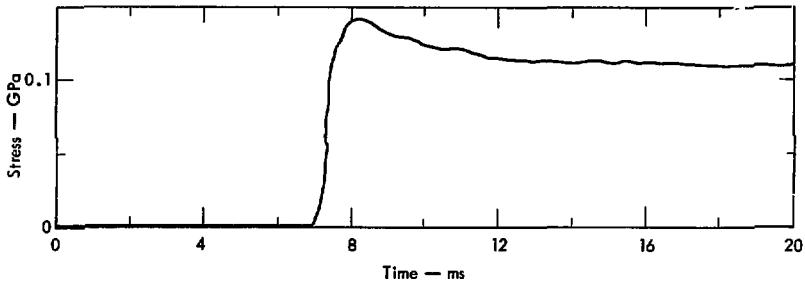

Fig. C-21. Stress history data from ST-B40T-B station. Horizontal range: 14.72 m; instrument range: 14.72 m; TOA: 7.0 ms; stress component: tangential; data: satisfactory. See Fig. B-2.

and the accelerometer was lost shortly after the shock wave reached the station. Again, cable breakage was the cause of failure.

Figure C-22 gives the TOA data from the backfill of the explosive. The plastic gage placed in that hole gave no data, as explained in Appendix A.

Figures C-23 through C-26 show acceleration and velocity data from the surface stations. The velocity gage at Ve-S25V-B

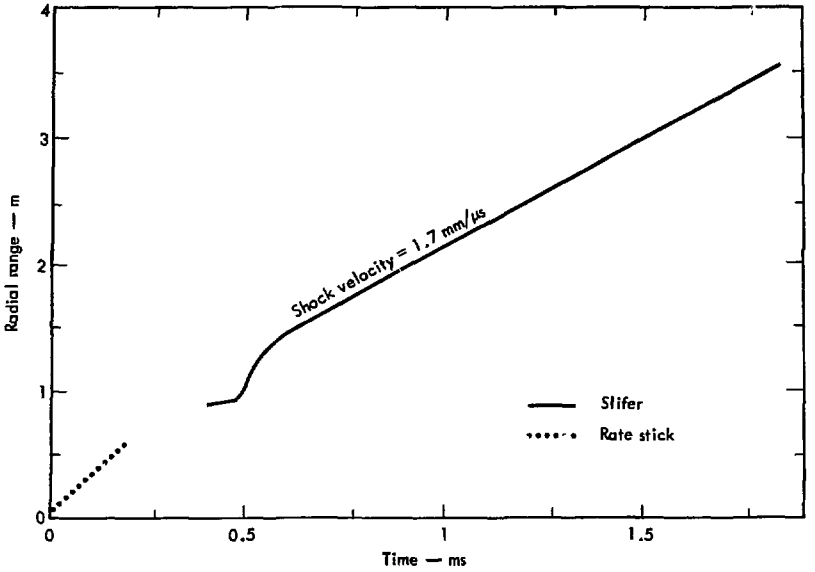

Fig. C-22. TOA data from the backfill.

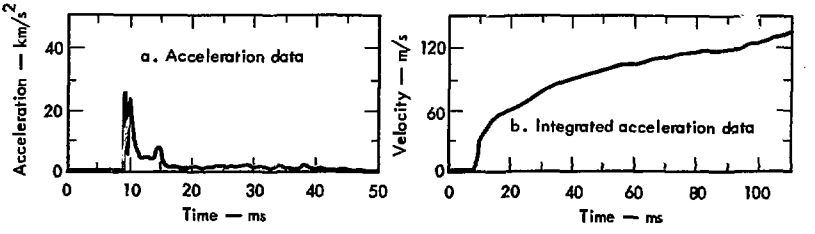

Fig. C-23. Acceleration and integrated acceleration data for Ac-S05V-B station. Horizontal range: 1.52 m; instrument range: 12.62 m; TOA: 9.3 ms; acceleration and velocity components: vertical. Acceleration data was satisfactory. However, a baseline shift in the acceleration signal quickly drove the integrated signal into the unbelievable range. If we stop the integration at 13 ms, we obtain a peak velocity of 58 m/s. See Fig. B-1b.

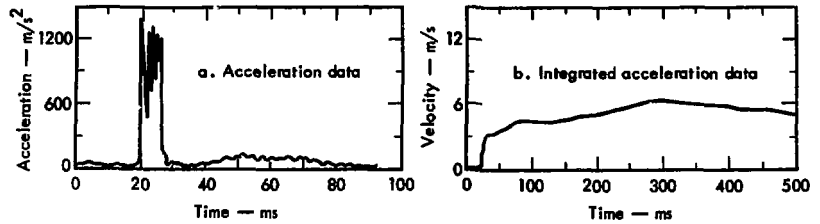

Fig. C-24. Acceleration and integrated acceleration data for Ac-S50HR-B station. Horizontal range: 13.53 m; instrument range: 18.41 m; TOA: 17.6 ms; acceleration and velocity component: horizontal radial. The acceleration data was poor. Although the range settings were satisfactory, the signal-to-noise ratio was fairly high. Most damaging, however, was a large amplitude ringing noise signal riding on top of the real signal. The noise was probably a result of poor coupling between the transducer and the ground surface, or possibly a poor grouting job. The integrated acceleration data was satisfactory. See Fig. B-1b.

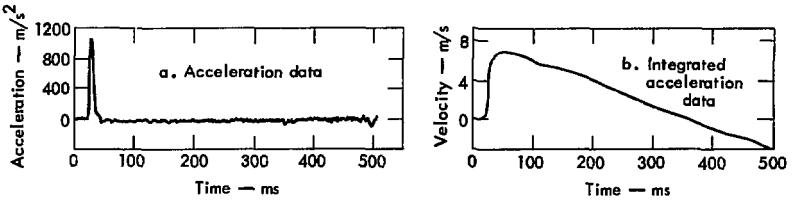

Fig. C-25. Acceleration and integrated acceleration data from Ac-S80V-B station. Horizontal range: 23.9 m; instrument range: 26.97 m; TOA: 22.9 ms; acceleration and velocity component: vertical; data: satisfactory. See Fig. B-1b.

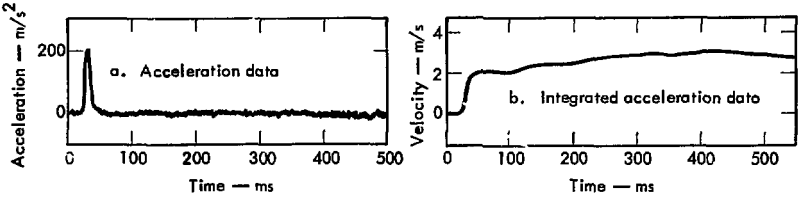

Fig. C-26. Acceleration and integrated acceleration data from Ac-S80HR-B station. Horizontal range: 23.9 m; instrument range: 26.97 m; TOA: 23.1 ms; acceleration and velocity component: horizontal radial; data: satisfactory. See Fig. B-1b.

station gave no data. Both carriers were dead before shot time. For some unexplainable reason, both carriers started again at ~500 ms. The lateness and the peculiar behavior make this data valueless. The velocity gage at Ve-S50V-B station also gave no data. Both carriers looked good throughout the entire time, and the subcarrier showed some modulation, but the data does not even resemble a signal. It is interesting that the accelerometer at this location also gave a poor signal.

STEMMED 6-m SHOT

Instrumentation for this shot was limited to rate sticks, a plastic gage, one slifer, and four surface motion stations. The rate sticks and the plastic gage were embedded in the HE sphere. The slifer extended from near the center of the HE sphere, through the top hemisphere of the HE, and up through the grout in the emplacement hole to the surface. The surface motion stations were located at 1.68, 7.62, 13.72, and 19.78 m from surface ground zero, as shown in Fig. 3.

Figure C-27 gives the detonation history of the explosive. The plastic gage gave no data, as explained in Appendix A. Figure C-28 gives the TOA data for the backfill.

Figures C-29 through C-32 give data from the surface stations. The velocity gages at Ve-S40V-C and Ve-S40HR-C stations gave no data. In the first case, the subcarrier failed sometime before the shot. In the second, both the main carrier and the subcarrier were present and operating, but the system gave no apparent signal during the shot.

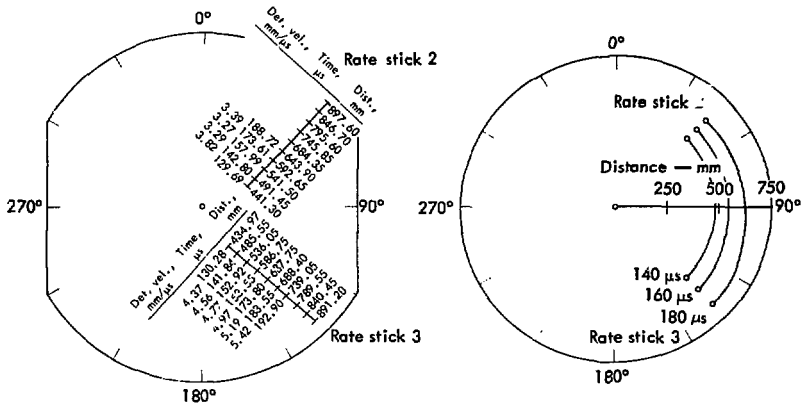

a. Detonation velocity and uniformity

b. Detonation symmetry

Fig. C-27. HE detonation history, DOIIA-3, 6 m, stemmed.

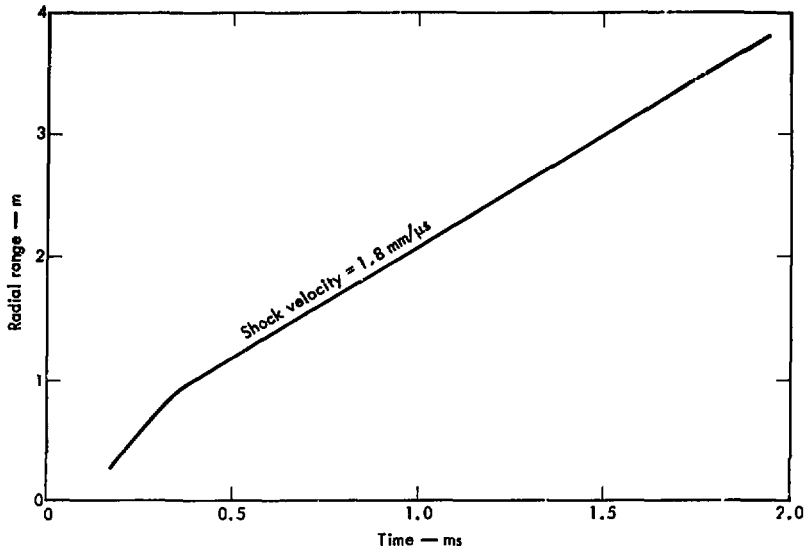

Fig. C-28. TOA data from the backfill.

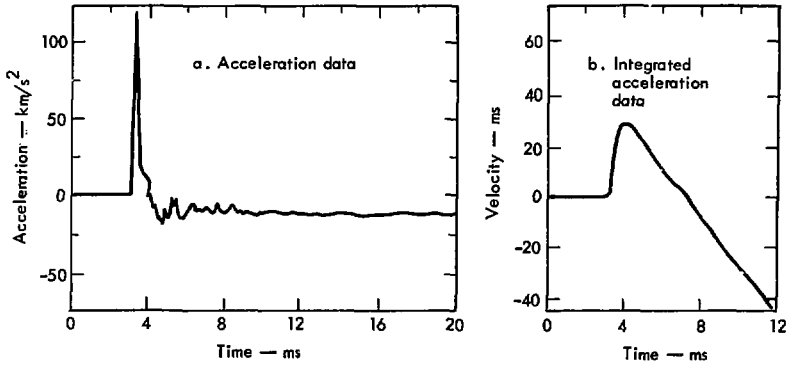

Fig. C-29. Acceleration and integrated acceleration data from Ac-S05V-C station. Horizontal range: 1.98 m; instrument range: 6.22 m; TOA: 3.20 ms; acceleration and velocity component: vertical. Acceleration signal was satisfactory to 4 ms, when the signal transmission system failed, giving a very pronounced baseline shift. Integrated acceleration data was very poor. See Fig. B-1b.

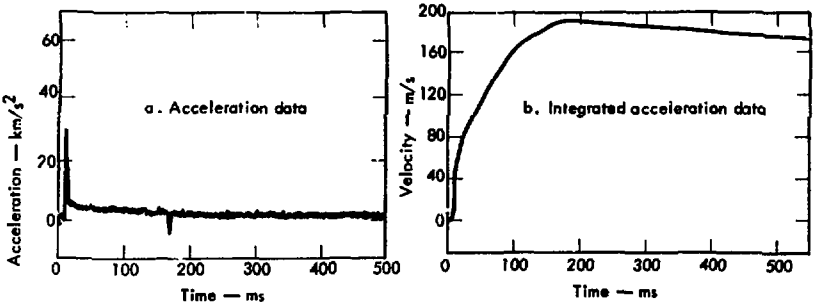

Fig. C-30. Acceleration and integrated acceleration data from Ac-S20V-C station. Horizontal range: 7.62 m; instrument range: 9.69 m; TOA: 5.6 ms; acceleration and velocity component: vertical. Acceleration data was very poor. The signal had a pronounced baseline shift and was very noisy; both situations originated from a mechanical failure somewhere in the system. Integrated acceleration data was questionable; it had a baseline correction that may not be correct. See Fig. B-1b.

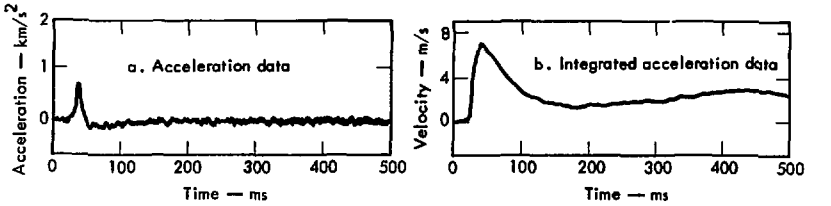

Fig. C-31. Acceleration and integrated acceleration data for Ac-S65V-C station. Horizontal range: 19.78 m; instrument range: 20.66 m; TOA: 25.0 ms; acceleration and velocity component: vertical; data: satisfactory. See Fig. B-1c.

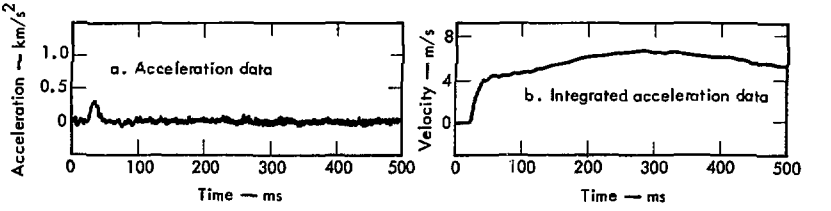

Fig. C-32. Acceleration and integrated acceleration data for Ac-S65HR-C station. Horizontal range: 19.78 m; instrument range 20.66 m; TOA: 25.7 ms; acceleration and velocity component: horizontal radial. Acceleration data was satisfactory, with very poor signal-to-noise ratio; integrated acceleration data was satisfactory. See Fig. B-1b.